LMSC-D057194

# UNSTEADY AERODYNAMIC FLOW FIELD ANALYSIS OF THE SPACE SHUTTLE CONFIGURATION

## Part IV: 747/ORBITER AEROELASTIC STABILITY

by
J. Peter Reding and Lars E. Ericsson
March 1976

Prepared Under Contract NAS 8-30652
for
National Aeronautic and Space Administration

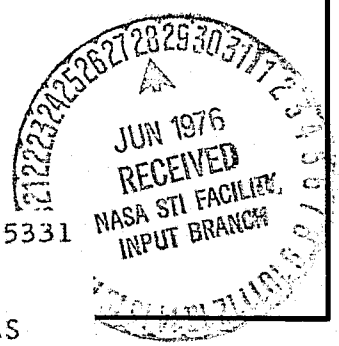




Lockheed MISSILES and SPACE COMPANY, INC.
SUNNYVALE, CALIFORNIA

# UNSTEADY AERODYNAMIC FLOW FIELD ANALYSIS OF THE SPACE SHUTTLE CONFIGURATION

## Part IV: 747/ORBITER AEROELASTIC STABILITY

by

J. Peter Reding and Lars E. Ericsson

March 1976

Prepared Under Contract NAS 8-30652

for

National Aeronautic and Space Administration

Lockheed Missiles & Space Company, Inc.
A Subsidiary of Lockheed Aircraft Corporation
Sunnyvale, California

## ABSTRACT

A quasi-steady analysis of the aeroelastic stability of the lateral (antisymmetric) modes of the 747/Orbiter vehicle has been accomplished. The interference effect of the orbiter wake on the 747 tail furnishes an aerodynamic undamping contribution to the elastic modes. Likewise, the upstream influence of the 747 tail and aft fuselage on the orbiter beaver-tail tail fairing also is undamping. Fortunately these undamping effects cannot overpower the large damping contribution of the 747 tail and the modes are damped for the configurations analyzed. However, significant interference effects of the orbiter on the 747 tail have been observed in the pitch plane. Thus, it is recommended that the stability of the pitch plane (symmetric) modes be analyzed. Furthermore, there was not sufficient data to analyze the upstream interference effects on the pointed tail fairing. If this is a viable configuration it should also be analyzed as the upstream effects will be larger and could cause overall aerodynamic undamping.

The high response of the 747 vertical tail in the orbiter wake has also been considered. Wind tunnel data point to flapping of the OMS pod wakes as the source of the wake resonance phenomenon.

CONTENTS

# ILLUSTRATIONS

Figure

ILLUSTRATIONS (Continued)

Figure

# Section 1
# INTRODUCTION

Analysis of the straight wing space shuttle booster (Refs. 1 and 2) indicated the possibility of aerodynamic undamping of the lateral (antisymmetric) free-free bending modes (Fig. 1). This was the result of aerodynamic interference of the orbiter wake on the booster tail. The orbiter-induced booster-tail-load for the various 747/Orbiter configurations (Fig. 2) is of the same order of magnitude as the interference load on the tail of the straight wing shuttle booster (Fig. 3). This causes some concern for the aeroelastic stability of the 747/Orbiter. Lockheed Missiles & Space Co. Inc., was given the task of applying the same quasi-steady techniques that were so successful in the aeroelastic analysis of the Apollo-Saturn (Refs. 3 and 4) to the 747/Orbiter. The following summarizes the results of this analysis. It should be emphasized that this analysis is dependent upon static aerodynamic data as an input and, therefore, is deficient where experimental data are not available. Refs. 5 and 6 are the sources of the aerodynamic data used.

## Section 2
## AERODYNAMIC INTERFERENCE EFFECTS

The orbiter effectively steers the flow forward of the 747 tail as illustrated in Fig. 4a. This steering induces a crossflow over the tail that is proportional to the orbiter yaw angle ($\beta_o$). The interference load, $\Delta^i C_{Y\beta w} \beta_o$ (t-$\Delta$t),* that results from the crossflow lags the orbiter by an amount of $\Delta\beta = \beta\Delta t$ where $\Delta t = (x_T - x_O)/\bar{U}$. $\bar{U}$ is the convection speed in the orbiter wake and $(x_T - x_O)$ is the distance from the orbiter base to the 747 tail. This wake directing effect is directly analogous to the wake directing effect of the Apollo escape rocket (Ref. 3).

In addition to the induced load on the 747 tail there is the usual local attitude ($\beta_T$) dependent load illustrated in Fig. 4. This load is simply ($C_{Y\beta s} \beta_T$) where

$$C_{Y_{\beta s}} = C_{Y_\beta} \quad (q_w/q_\infty) \tag{1}$$

$C_{Y\beta}$ is the tail effectiveness in the free stream (orbiter off), and $q_w/q_\infty$ is the wake to free stream dynamic pressure ratio. The dynamic pressure ratio has been successfully related to the aerodynamic coefficient ratio. In the case of the Apollo-Saturn the axial force ratio was found to be indicative of the dynamic pressure ratio, i.e., $q_w/q_\infty = C_{Aow}/C_{Ao}$. However, this is not an effective indicator for the 747 tail since differences in the tail increments between orbiter on and orbiter off approach the magnitude of the data accuracy. The rudder effectiveness was judged to be a better indicator of the dynamic pressure ratio, thus $q_w/q_\infty = C_{Y\delta w}/C_{Y\delta}$ (Fig. 5).

---

*The interference derivative, $\Delta^i C_{Y\beta T} = (C_{Y\beta T})_{747/O} - (C_{Y\beta T})_{747}$ has been non-dimensionalized to the tail area ($S_T$) rather than the wing ($S_W$) to furnish a valid basis for comparison of the relative magnitude of the interference effects.

The total orbiter side force derivative on the tail is the sum of induced and local derivatives,

$$C_{Y_\beta} = C_{Y_{\beta_S}} + \Delta^i C_{Y_{\beta_W}} \tag{2}$$

The convection velocity ratio is simply

$$\bar{U}/U_\infty = (q_w/q_\infty)^{1/2} \tag{3}$$

Although this tacitly assumes incompressible flow it was found to give a good approximation to the measured Apollo escape rocket wake convection speed (Ref. 7). This is probably because the bulk of the wake flow is of low speed and hence incompressible. This should be an even better estimate for the slender 747 tail since it is almost completely buried in the low velocity wake core.

The local and induced load components for the various 747/Orbiter configurations are presented in Fig. 6. The induced and local tail derivatives are approximately equal and opposite at least at the higher subsonic Mach numbers.

## Section 3
## AERODYNAMIC DAMPING

The equation of motion of an elastic vehicle describing single degree of freedom bending oscillations can be written as follows (Refs. 2 and 3),

$$\ddot{q}(t) + 2\omega \left[\zeta - \frac{B}{2\omega U}(D_s + D_a)\right] \dot{q}(t) + \omega^2 \left[1 - \frac{B}{\omega^2}(K_s + K_a)\right] q(t) = f(t) \qquad (4)$$

where $B = \rho U^2 S/2\tilde{m}$ and $f(t)$ is the buffeting force input. $D_s$ and $D_a$ are the aerodynamic damping derivatives for separated and attached flow respectively, where a negative value denotes damping. Multiplication by $\frac{-B}{2\omega U} = -\rho US/4\omega\tilde{m}$ puts the aerodynamic damping into the same form as the structural damping factor. The mode is stable if the $\dot{q}$-coefficient is positive, i.e

$$\zeta - \frac{B}{2\omega U}(D_s + D_a) \geq 0 \qquad (5)$$

The separated flow damping derivative $D_s$ for the 747/Orbiter is the sum of local and induced loads on the 747 tail and has been derived from Ref. 3 using the coordinate system of Fig. 7,

$$D_s = -C_{Y_{\beta_s}} \left[\phi(\xi_T)\right]^2 - \Delta^i C_{Y_{\beta_w}} \phi(\xi_T)\, \phi'(\xi_O)\, \frac{U}{\omega} \sin(\omega\Delta t) \qquad (6)$$

The attached flow damping derivative $D_a$ is obtained from first order momentum theory (Ref. 8), modified by use of the experimental values of $C_{Y_\beta}$ for both orbiter and 747 (Refs. 2 and 3). From Eq. (6) and Fig. 7 one can see that the contribution of the induced derivative to $D_s$ is undamping (positive) for the positive, statically stabilizing $\Delta^i C_{Y\beta_W}$ since $\phi(\xi_T)$ and $\phi'(\xi_O)$ have opposite signs. This is illustrated in Fig. 8.

Consider the orbiter and 747 tail deflected in some mode as shown in the upper sketch. By virtue of its yaw angle ($\beta_O$) the orbiter induces a load on the 747 tail ($\Delta^i C_{Y\beta w}\ \beta_O$) that tends to return the tail to its null position. The interference effect is, therefore, statically stabilizing. As the orbiter and tail passes through the null position during the modal oscillation a residual load occurs on the tail, $\Delta^i C_{Y\beta w}$ $\beta_O$ (t-$\Delta$t), that was generated at an earlier time (t-$\Delta$t) when the orbiter yaw angle was $\beta_O$ (t-$\Delta$t). This residual load is in the direction of motion, thus driving the oscillation, i.e., it is undamping.

The 747 tail and aft fuselage have an interference effect on the orbiter tail fairing through the wake recirculation region that is similar to dynamic sting interference (Refs. 9 and 10). Actually, three interference loads occur on the bulbous base (Fig. 9). The first, a forebody crossflow effect, is analogous to the crossflow effect for a slender conic forebody where forebody crossflow thickens the leeside boundary layer (Fig. 9a). The leeside wake separation point moves forward in response to the boundary layer thickening and a negative, statically destabilizing, tail load is generated. The load lags the body motion due to the finite time required to convect a disturbance from nose to tail within the boundary layer. A similar effect results on the shuttle orbiter due to yaw. However, in this case it is the strength of the vortex generated at the strake apex that dominates the aft body flow (Ref. 11). The vortex tends to strengthen the fuselage boundary layer by entraining high energy free stream flow into the boundary layer. At $\beta \neq 0$ the leeward vortex is swept away from the fuselage; thus, the leeside boundary layer is weakened allowing the separation to move upstream. The converse occurs on the windward side resulting in a positive, statically destabilizing load. Thus, the effect is to increase the orbiter yaw damping.

There are two upstream effects in the free wake effect. The first effect occurs because when the forebody generates lift the wake immediately behind the body is inclined relative to the free stream, (Fig. 9b). Thus, a pressure gradient exists across the wake that eventually turns it parallel to the free stream. The pressure gradient produces higher windward side wake neck pressures that, when convected upstream through the wake recirculation region, cause a separation asymmetry. The result is a statically stabilizing tail load which, of course, is undamping. The final

induced load is analogous to the sting interference effect on a bulbous based re-entry body (Fig. 9c and Refs. 9 and 10). The sidewash of the orbiter wake over the 747 tail results in unequal windward and leeward side wake neck pressures which, when convected forward through the wake recirculation region, cause a separation asymmetry and an induced load on the tail fairing. The sense of this induced load depends upon the inclination of the tail relative to the orbiter ($\beta_T$). The upstream effects have a very long time lag as they involve convection downstream from the orbiter to the 747 tail and then upstream through the low velocity recirculation region, (Refs. 9 and 10) i.e.

$$\Delta t = c\,(\xi_T - \xi_O)\left(\frac{1}{\overline{U}} + \frac{1}{\overline{U}_u}\right) \tag{7}$$

where $\overline{U}$ and $\overline{U}_u$ are the downstream and upstream communication velocities respectively.

In Fig. 10 the loads on the T.C.5 (beaver-tail) tail cone for orbiter alone at $\alpha = 8$ and 15 degrees are compared with the 747/Orbiter with a total orbiter inclination ($I + \alpha$) of 14 degrees.* One would expect the 747/Orbiter measurements to fall between these two orbiter alone curves. The reason it doesn't is undoubtedly due to interference effects from the 747. The orbiter alone model was tested on a strut support, thus avoiding sting interference effects (Ref. 5). The differences between orbiter alone and 747/Orbiter can be explained by reference to the flow sketches in Fig. 10. For the orbiter alone the tail cone experiences only a minor flow separation. The dominant load is ahead of the separation on the attached flow portion of the tail fairing. This negative, attached flow, derivative ($C_{Y_a}$) is stabilizing. It is augmented by the free wake effect ($\Delta^i C_{Y_W}$) and opposed by the destabilizing forebody crossflow induced effect ($\Delta^i C_{Y_{XF}}$). The negative derivatives ($C_{Y_a}$ and $\Delta^i C_{Y_W}$) dominate $(\Delta C_Y)_{TC}$. However $\Delta^i C_{Y_{XF}}$ effectively cancels the effects of $C_{Y_a}$ and $\Delta^i C_{Y_W}$ on the yawing moment $(\Delta C_n)_{TC}$. Thus, the yawing moment is essentially zero.

*$(C_\beta)_{TC} = (C_\beta)_{O+TC} - (C_\beta)_O$ where TC denotes tail cone and O orbiter.

The 747 tail and aft fuselage add the upstream communication effect $\Delta^i C_{Y_T}$ (Fig. 9c) and also have the effect of increasing the size of the separation thus diminishing $C_{Y_a}$. Experience (Ref. 9) has shown that at low Mach numbers ($M \leq .3$) upstream effects can be neglected ($\Delta^i C_{Y_W} \approx \Delta^i C_{Y_T} \approx 0$). Thus, forebody boundary layer effects will dominate the tail fairing load, and an overall positive $\left(\Delta C_{Y_\beta}\right)_{TC}$ and negative $\left(\Delta C_{n_\beta}\right)_{TC}$ will result. As Mach number is increased from $M = .3$ the upstream wake effects ($\Delta^i C_{Y_W}$ and $\Delta^i C_{Y_T}$) grow causing the observed nonlinearities of $\left(\Delta C_{Y_\beta}\right)_{TC}$ and $\left(\Delta C_{n_\beta}\right)_{TC}$ with Mach number. In order to conduct an aeroelastic analysis of the tail fairing one must know the various component loads on the tail fairing that are associated with different time lags. Specifically $C_{Y_{\beta a}}$ and $\Delta^i C_{Y_{\beta XF}}$ must be known separately as their time lags are different (no time lag for $C_{Y_{\beta a}}$ and the boundary layer convection lag for $\Delta^i C_{Y_{\beta XF}}$). Although $\Delta^i C_{Y_{\beta W}}$ and $\Delta^i C_{Y_{\beta T}}$ have the same time lag (downstream-upstream through the wake recirculation region) they must be known separately since for the elastic body the damping effect of the latter is proportional to $\phi'(\xi_T) - \phi'(\xi_O)$ whereas the former is a function of $\phi'(\xi_O)$ only (Fig. 7). The nonlinearities of orbiter alone and 747/Orbiter $\left(\Delta C_{n_\beta}\right)_{TC}$ curves (Fig. 10) are indicative of $\Delta^i C_{n_{\beta W}}$ and $\Delta^i C_{n_{\beta W}} + \Delta^i C_{n_{\beta T}}$ respectively. However, sufficient information is not available to separate $C_{n_{\beta a}}$ and $\Delta^i C_{n_{\beta XF}}$. The assumption was made that the difference between orbiter alone at $\alpha = 15°$ and 747/Orbiter yawing moments was indicative of $\Delta^i C_{n_{\beta XF}}$. Admittedly this is an underestimate of $\Delta^i C_{n_{\beta XF}}$. However, since $\Delta^i C_{n_{\beta XF}}$ is damping the assumption is conservative.

The contribution of these induced tail cone loads to the damping was derived from Refs. 9 and 10.

$$
\left.
\begin{aligned}
D_{TC} = {} & \Delta^i C_{n_{\beta XF}}\, b \left[\phi'(\xi_O)\right]^2 \frac{U}{\omega} \sin\left[\frac{\omega}{U}(\xi_O - \xi_A)\, c\right] \\
& + \Delta^i C_{n_{\beta T}}\, b\, \phi'(\xi_O) \left[\phi'(\xi_O) - \phi'(\xi_T)\right] \frac{U}{\omega} \sin\left[\gamma \ell \left(\frac{\omega}{U}\right)\right] \\
& + \Delta^i C_{n_{\beta W}}\, b\, \phi'(\xi_O)^2 \frac{U}{\omega} \sin\left[\gamma \ell \left(\frac{\omega}{U}\right)\right]
\end{aligned}
\right\} \qquad (8)
$$

where b is the reference length (747 span)

$\gamma$ is the wake time lag taken from Ref. 10 and referenced to the body diameter.

Before presenting the results of the aeroelastic analysis it is appropriate to first discuss the limitations of the quasi-steady theory.

The lumped-time-lag, quasi-steady, theory assumes that dynamically the instantaneous load distribution on a submerged body element is not substantially different from the static load distribution. It is not particularly significant how many cycles occur between the interference source and the submerged body unless other body elements are present that could alter the interference effect. This can be visualized from considering Fig. 11. The submerged 747 tail in Figure 11a is well aft of the orbiter and submerged in the orbiter wake. The tail load can be expressed as a single lumped load since the pertinent tail dimension c is small relative to the wavelength of the oscillating wake, $\lambda$. However, when $\lambda \rightarrow c$ (Fig. 11b) one can see that the wake induced crossflow at the rear of the tail will be altered by conditions at the leading edge, and the quasi-steady technique breaks down. Thus, as long as $c/\lambda \leq .25$ the wave distortion will be minimal and the quasi-steady theory is valid. This limit of the quasi-steady theory is presented in Fig. 12 for the four antisymmetric modes of the 747/Orbiter that have been analyzed. Of course, this limit is not rigid and the results will gradually deteriorate as one goes deeper into the questionable region (as $c/\lambda$ increases).

# Section 4
# DISCUSSION OF RESULTS

The equivalent elastic body damping derivatives have been computed for the four modes in Figure 13. All modes experience an undamping contribution from the interference effect of the orbiter on the 747 tail (Fig. 14). Modes 4 and 12 experience an undamping contribution from the orbiter tail fairing.

Although the orbiter induced damping derivative $\Delta^{i}D_{\nu W}$ is undamping the effect of local crossflow on the 747 tail $D_{\nu S}$ is highly damping. The surprising result is that the local cross flow effect is so large that the orbiter interference is almost insignificant in comparison (Fig. 15). Why the orbiter induced effect is so overpowered by the local cross flow for the 747/Orbiter, although it dominated the damping of the straight wing booster, can be seen from a comparison of mode shapes (Fig. 16). The relative deflection of 747 tail is three times that of the straight wing orbiter. Since the local damping of the tail is a function of the square of the modal deflection at the tail, Eq. (6), the 747 tail is an order of magnitude more effective as a damper. Thus, the 747 tail local damping derivative is an order of magnitude larger than the orbiter induced undamping effect, resulting in overall damping.

Figure 17 illustrates the effects of the various damping components. Note that the undamping of the tail fairing is significant at high speeds whereas it is insignificant at low speeds. However, it definitely effects the shape of the damping curve. In Figures 18 and 19, the damping of the four antisymmetric modes for the various configurations are shown for the two critical flight conditions (ferry and orbiter launch). Although the ferry results may be somewhat questionable for the higher modes (Figures 18a and 18b), they still indicate that these modes will be damped.

It should be emphasized that for only one configuration (T.C.5, I = 8°, AT38.3) was there sufficient static data to allow an estimate of the tail fairing effects. This is particularly important if the pointed T.C. 4 tail fairing (or something similar) is a viable candidate, as it will be more sensitive to upstream effects. Considering the large effect on the beavertail tail fairing it is very possible that the T.C. 4 fairing could cause undamping of one or more antisymmetric modes. Certainly it is potentially more dangerous.

No estimate has yet been made of the damping of any of the symmetric or pitch plane modes. Comparison of 747 horizontal tail normal force increments indicate a significant downwash effect of the orbiter on the horizontal tail (Fig. 20). The effect of orbiter downwash is of the same order of magnitude as the vertical tail effect (compare Figs. 20 and 6), hence interference effects could have significant dynamic effects unless the symmetric modes are also dominated by local crossflow effects at the tail. However, the effect of the tail fairing seems the most likely potential threat to the damping of the symmetric modes. The interference effects on the beaver-tail tail fairing should be significantly greater in the pitch plane than it was in the yaw plane due to its flat configuration. Thus, it could cause significant aerodynamic undamping. It certainly warrants further analysis.

# Section 5
# 747 TAIL RESONANCE

Up until now the discussion has been concerned only with the left hand side of Eq. (4). The right hand side, the buffeting force input, has been observed to have a significant effect on the 747 tail mode response. Subscale response measurements reveal a resonance with the orbiter wake (Ref. 12). Fortuitously, the resonance occurs at a reduced frequency of $\omega\ell/U = .2$ based on the orbiter width, (compare Figs. 21 and 22). There is no apparent physical reason why the characteristic frequency of the three dimensional orbiter wake should correspond to the frequency associated with the wake of a two dimensional cylinder. When the frequency spectra of the tail response and the fluctuating velocity ratio are nondimensionalized using the OMS pod width, d, as the characteristic length the peaks agree well with Roberts wake flapping frequency $\omega d/U = .135$ (Ref 13 and Figs. 23 and 24). Of course this is not conclusive since within the experimental precision, $\omega d/U = .135$ and $\omega\ell/U = .2$ predict the characteristic frequency equally well. However, it does make the OMS pod wake a viable candidate to be the source of the velocity fluctuations. The remainder of the data (the success or non-success of the fixes tried to reduce the tail response and velocity fluctuation) gives further evidence in favor of the OMS pod wake being the source.

The fluctuating velocity profiles at various stations in the orbiter wake indicate that the source of the maximum overall velocity fluctuations is in the region of the OMS pods (Fig. 25). The success of the scoops (positioned behind the gap between the OMS pods and the orbiter vertical tail) in reducing both the 747 tail response (Figs. 21 and 23) and the velocity fluctuations (Fig. 26) give further evidence that the OMS pod flow effects both the maximum overall velocity fluctuations and their characteristic frequency. Speed brake deflection has a similar effect (Fig. 27). The oil flow photographs in Fig. 28 indicate that speed brake deflection affects the flow over the OMS pod (Ref. 14). The effect is in a direction that would move the OMS wake

downward to mix with the main orbiter wake and move it outward away from the 747 tail. The wake from the speed brake itself could also stabilize the OMS pod wake through mixing.

One might also suspect that the speed brake reduces the velocity fluctuations by reducing the mean wake velocity gradient, $d\,(V_{mean}/V_\infty)/dz$, in the wake. All the velocity data presented to date show a correlation between the vertical location of the maximum overall fluctuating velocity ratio and the maximum slope of the mean velocity gradient. This correlation breaks down, however, when the tail cone is added (Fig. 27). The tail cone eliminates the separate pod and orbiter base wakes and creates a diminutive single wake.* However, the velocity gradients remain about the same. They may even increase slightly. Still, the magnitude of the overall fluctuating velocity ratio is substantially decreased, and the location of its maximum does not correlate with the maximum mean velocity gradient. Thus, the mean velocity gradient does not appear to be the cause of the high velocity fluctuations.

Deflection of the body flaps contracts the orbiter wake vertically, thus reducing the peak values of $(V_{RMS}/V_\infty)^2$. However, the resonant peak is not eliminated as it is with speed brake deflection or with the scoops (Fig. 29). The body flap does not effect the OMS pod wakes directly; it simply facilitates mixing with the main orbiter wake, thus accelerating the decay of the velocity fluctuations caused by the OMS pod wake.

The foregoing arguments do not conclusively prove that the OMS pod wake flapping is the source of the velocity fluctuations that drive the 747 tail. However, the evidence strongly supports this contention.

*At the low Mach number - Reynolds number conditions of the present tests.

# Section 6
# CONCLUSIONS

A quasi-steady analysis of the aeroelastic stability of four antisymmetric modes of the 747/Orbiter has shown that the modes are aerodynamically damped for the following configurations,

1. 747/Orbiter without tail fairing
2. 747/Orbiter with T.C. 5 (beaver-tail) tail fairing

The analysis indicates that the interference effect of the orbiter on the 747 tail, and the upstream effect of the 747 tail and aft fuselage on the orbiter tail fairing, have an aerodynamic undamping influence on certain critical modes. Fortunately, the large modal deflection of the 747 tail causes the damping effect of the 747 tail to overpower these undamping effects for the modes analyzed. However, because of insufficient static aerodynamic data, it was impossible to determine the upstream interference on the pointed (T.C. 4) tail cone. This could have an undamping effect on the antisymmetric modes that is significantly larger than for the beaver-tail tail fairing. Thus, if this is a viable configuration an aeroelastic analysis should be done, even though it requires obtaining further static wind tunnel data.

The available wind tunnel data indicate a significant orbiter interference effect on the horizontal tail of the 747. Likewise, the upstream interference effects on the tail fairing could be large (this is particularly true for the beaver-tail tail fairing). Thus, it is recommended that the aeroelastic stability of the symmetric modes be analyzed.

Available wind tunnel data indicate that the OMS pod wake flapping is probably responsible for the high response of the 747 tail in the orbiter wake. Thus, scoops, speed brake deflection, addition of a tail fairing or any other technique that alters, stabilizes, or eliminates the OMS wake will also eliminate the undesirable tail response.

# REFERENCES


1 Reding, J.P., and Ericsson, L.E., "Review of Delta Wing Space Shuttle Vehicle Dynamics," LMSC/D243938, October 1971.

2. Reding, J.P., and Ericsson, L.E., "Unsteady Aerodynamics Could Dominate the Space Shuttle Booster Aeroelastic Stability," AIAA Paper No. 74-362, Presented at AIAA/ASME/SAE 15th Structures, Structural Dynamics and Materials Conference, Las Vegas, Nevada, April 17-19, 1974.

3. Ericsson, L.E., and Reding, J.P., "Analysis of Flow Separation Effects on the Dynamics of a Large Space Booster," J. Spacecraft and Rockets, Vol. 2 No. 6, July-Aug 1962, pp. 481-490.

4. Ericsson, L.E., and Reding, J.P., "Report on Saturn I - Apollo Unsteady Aerodynamics, LMSC/A650215, Feb. 1964.

5. Anon., "Results of a 0.03 S cale Aerodynamics Investigation of a Boeing 747 Carrier (Model No. AX1319-I-1) mated with a Space Shuttle Orbiter (Model 45-0) Conducted in the Boeing Transonic Wind Tunnel (A5)," NASA CR-141, 800, August 1975.

6. Unpublished wind tunnel data for a 747 Carrier/Orbiter Configuration.

7. Reding, J.P., "Partial Simulation of Elastic-Body Dynamics for the Upper Stage Apollo-Saturn Launch Vehicle," LMSC M-37-67-4, Dec. 1967.

8. Bisplinghoff, R.L., Ashley, H. and Halfman, R.L., Aeroelasticity, Cambridge, Mass. Addison-Wesley, 1952, pp 418-419.

9. Ericsson, L.E., and Reding, J.P., "Aerodynamic Effects of Bulbous Bases," NASA CR-1339, August 1969.

10. Reding, J.P., and Ericsson, L.E., "Dynamic Support Interference," J. Spacecraft and Rockets, Vol. 9, No. 7, July 1972, pp. 547-553.

11. Reding, J.P., and Ericsson, L.E., "Unsteady Aerodynamic Flow-Field Analysis of the Space Shuttle Configuration," Part II Launch Vehicle Aeroelastic Analysis," LMSC/D057194, April 1976.

12. Young, J.C., "Partial Results of an Exploratory Experiment to Change the Dynamic Character of the Orbiter Wake, NASA JSC EX33-P117," August 1972.

13. Roberts, J.B., "Coherence Measurements in an Axisymmetric Wake," AIAA Journal,Vol. 11, No. 11, Nov. 1973, pp. 1569-1571.

14. Nichols, M.E., "Results of Investigations on the 0.004 Scale Model 74-U of the Configuration 4 (Modified) Space Shuttle Vehicle Orbiter in the NASA MSFC 14-by-14-Inch Transonic Wind Tunnel (OA 131)," NASA CR 141, 521, March 1975.

# Appendix A
## NOMENCLATURE

| | |
|---|---|
| A | axial force; coefficient $C_A = A/\rho U^2 S/2)$ |
| B | $\rho U^2 S/2\ \tilde{m}$ |
| b | wing span |
| c | reference length (mean aerodynamic chord) |
| D | damping derivative |
| d | OMS pod width |
| f(t) | buffeting force input |
| K | spring constant |
| $\ell$ | orbiter base width |
| M | Mach number |
| $\tilde{m}$ | generalized mass |
| n | yawing moment; coefficient $C_n = n/(\rho U^2 S\ b/2)$ |
| q(t) | normalized coordinate |
| S | reference area |
| t | time |
| U, $V_\infty$ | free stream velocity |
| $\bar{U}$ | convection velocity |
| V | local velocity |
| x | axial coordinate |
| Y | yaw force; coefficient $C_Y = Y/(\rho U^2 S/2)$ |

| | |
|---|---|
| z | lateral coordinate |
| $\alpha$ | angle of attack |
| $\beta$ | yaw angle |
| $\gamma$ | wake time lag |
| $\Delta$ | increment |
| $\delta$ | relative deflection; linear or angular |
| $\lambda$ | wavelength |
| $\xi$ | nondimensional axial coordinate, $\xi = x/c$ |
| $\zeta$ | structural damping as a fraction of critical |
| $\omega$ | circular frequency |
| $\phi$ | modal deflection |
| $\phi'$ | mode slope |

Subscripts

| | |
|---|---|
| A | strake apex |
| a | attached flow |
| O | orbiter base |
| RMS | root-mean-square |
| s | separated flow |
| T | 747 tail |
| TC | tail cone |
| u | upstream |
| W | wing |
| w | wake |
| XF | cross flow |
| $\nu$ | denotes local damping |

Subscripts (Continued)

| | |
|---|---|
| $\infty$ | free stream |
| 0 | $\beta = 0$ |
| 747 | denotes 747 |

Superscripts

| | |
|---|---|
| i | induced, e.g., $\Delta^{i}C_{Y} \equiv$ separation induced side force coefficient. |

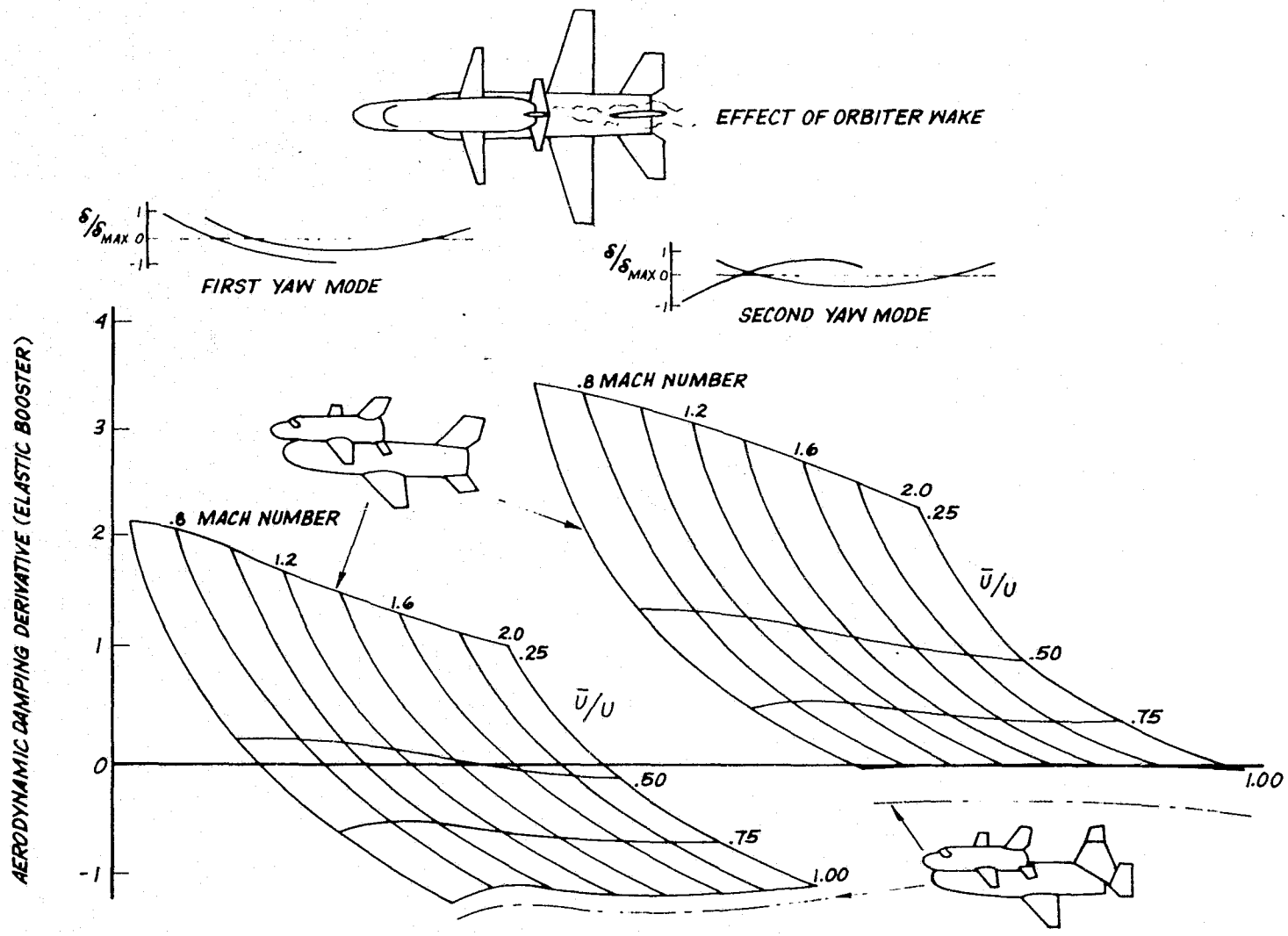


Figure 1 Yaw Damping of Straight Wing Booster

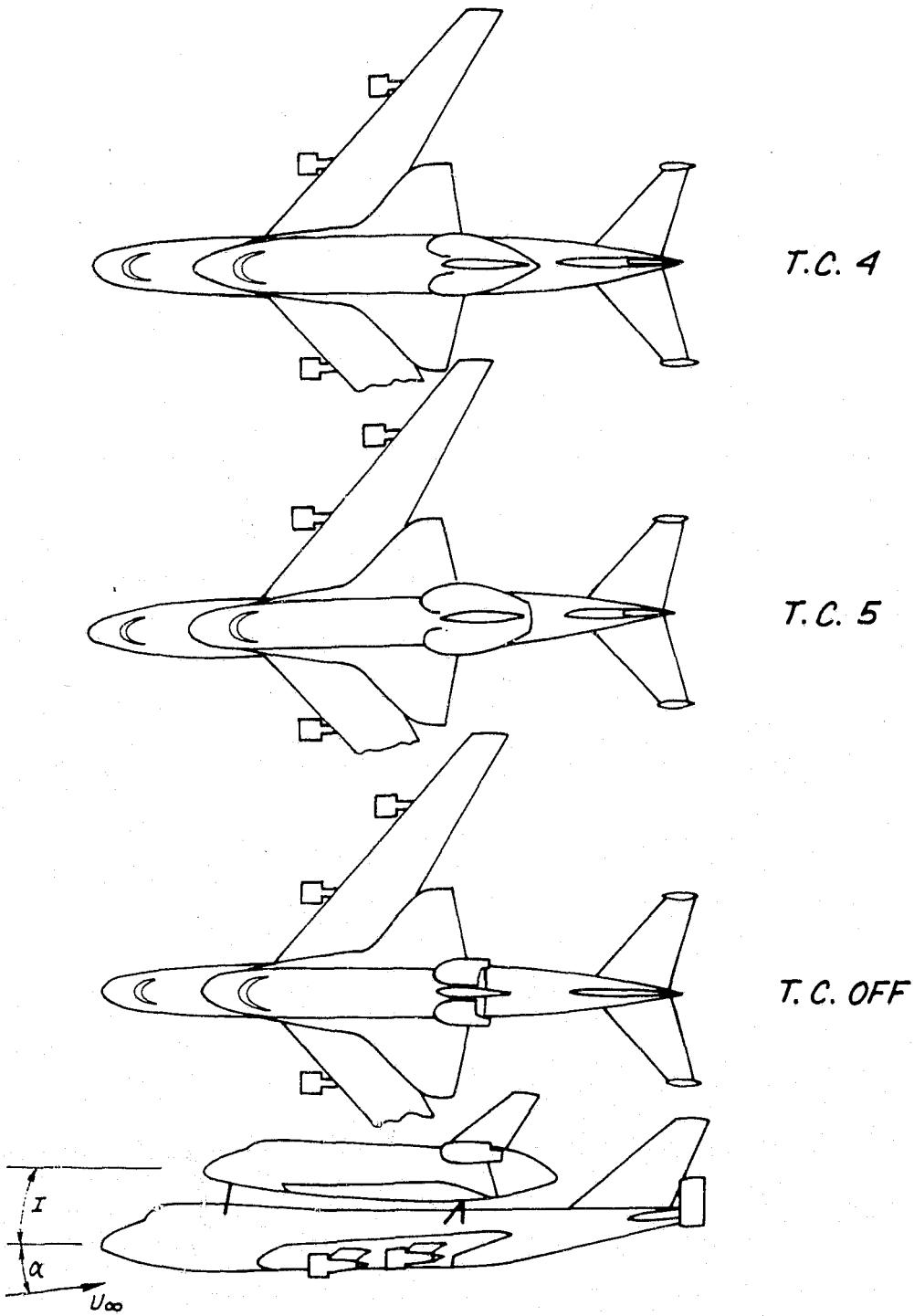


Figure 2 747/Orbiter Configurations

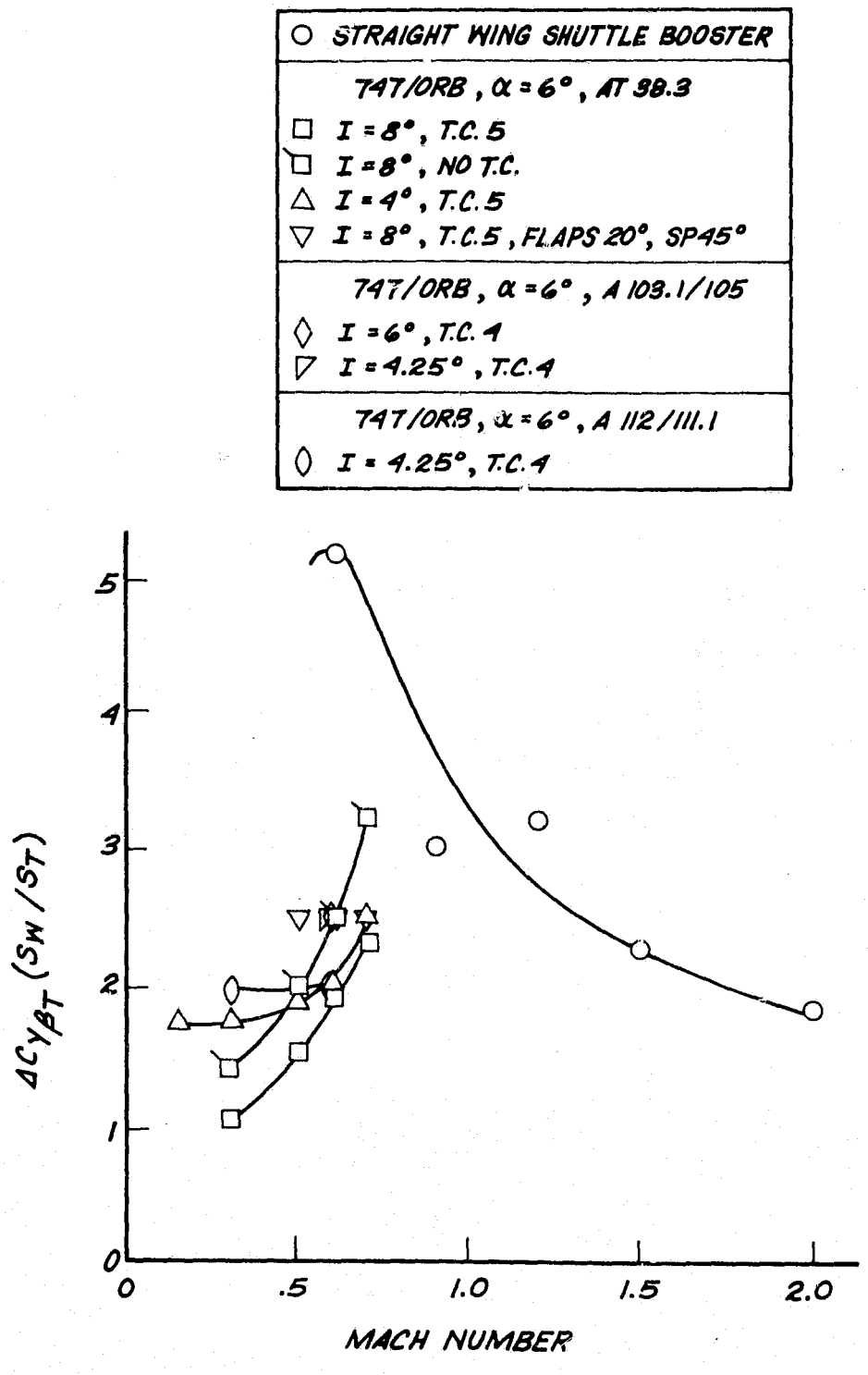


Figure 3 Effect of Orbiter Wake on Carrier Vehicle Trail Loads

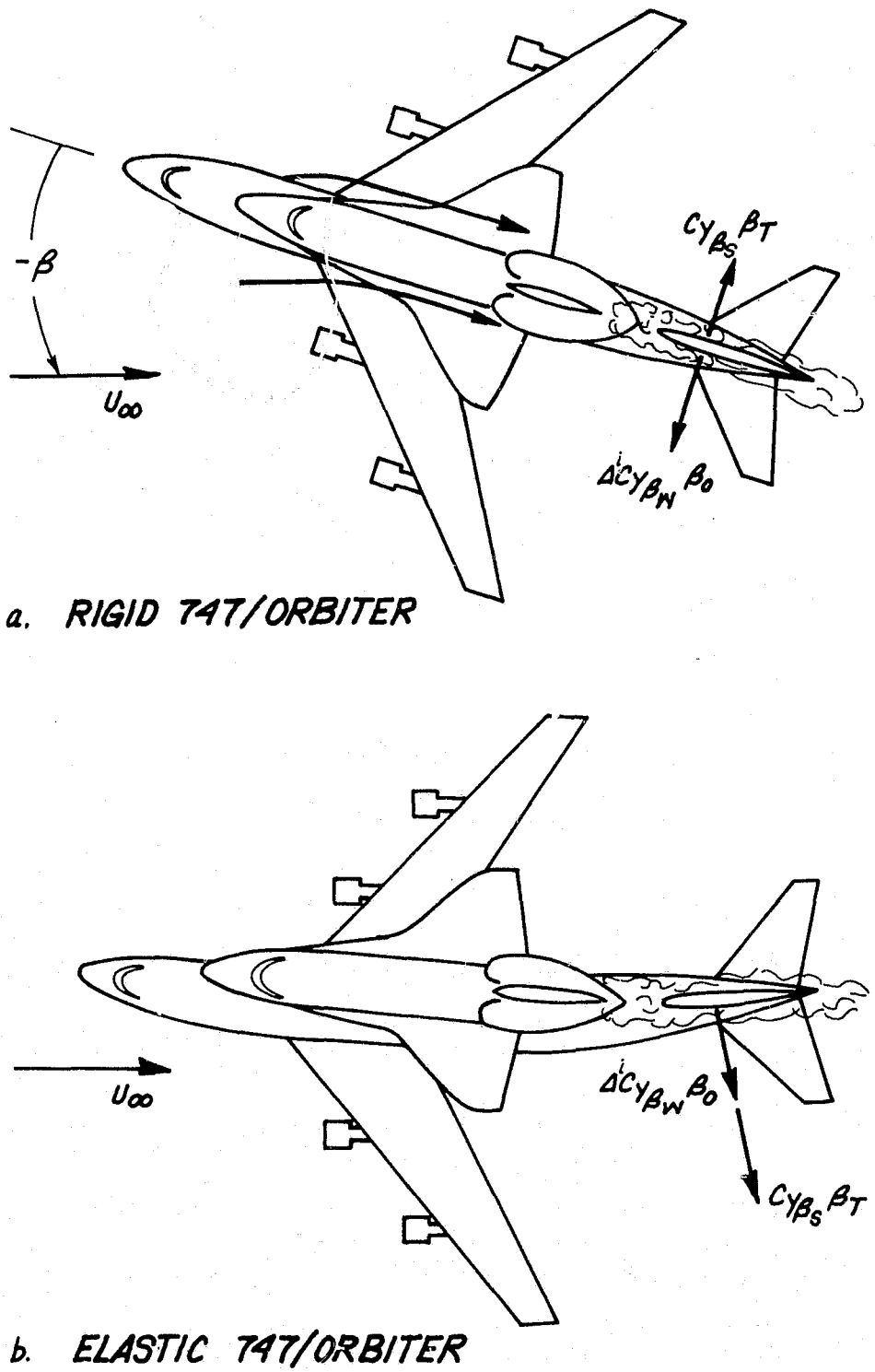


Figure 4 747/Orbiter Aerodynamic Interference

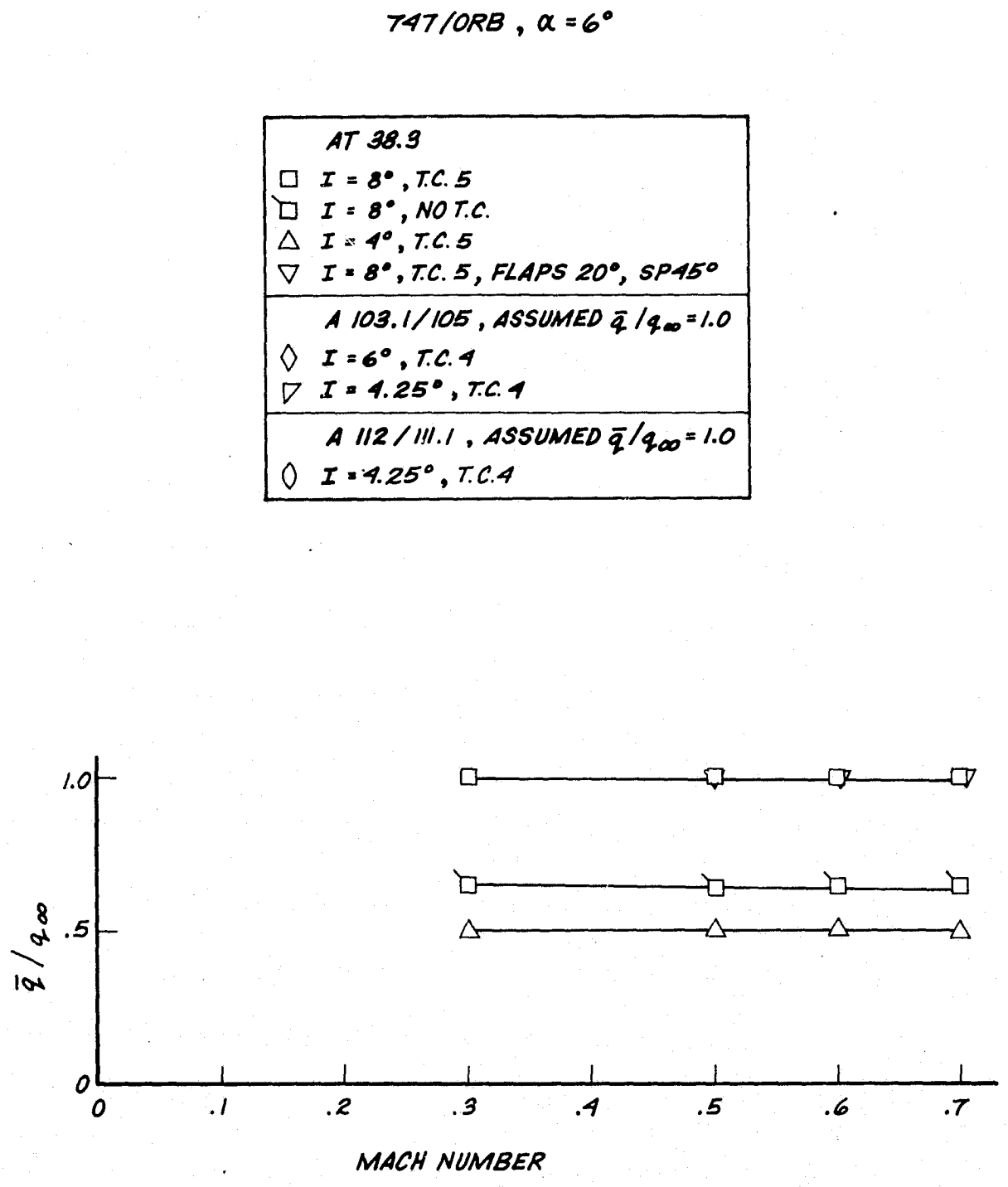


Figure 5 Average Dynamic Pressure Ratio in Orbiter Wake

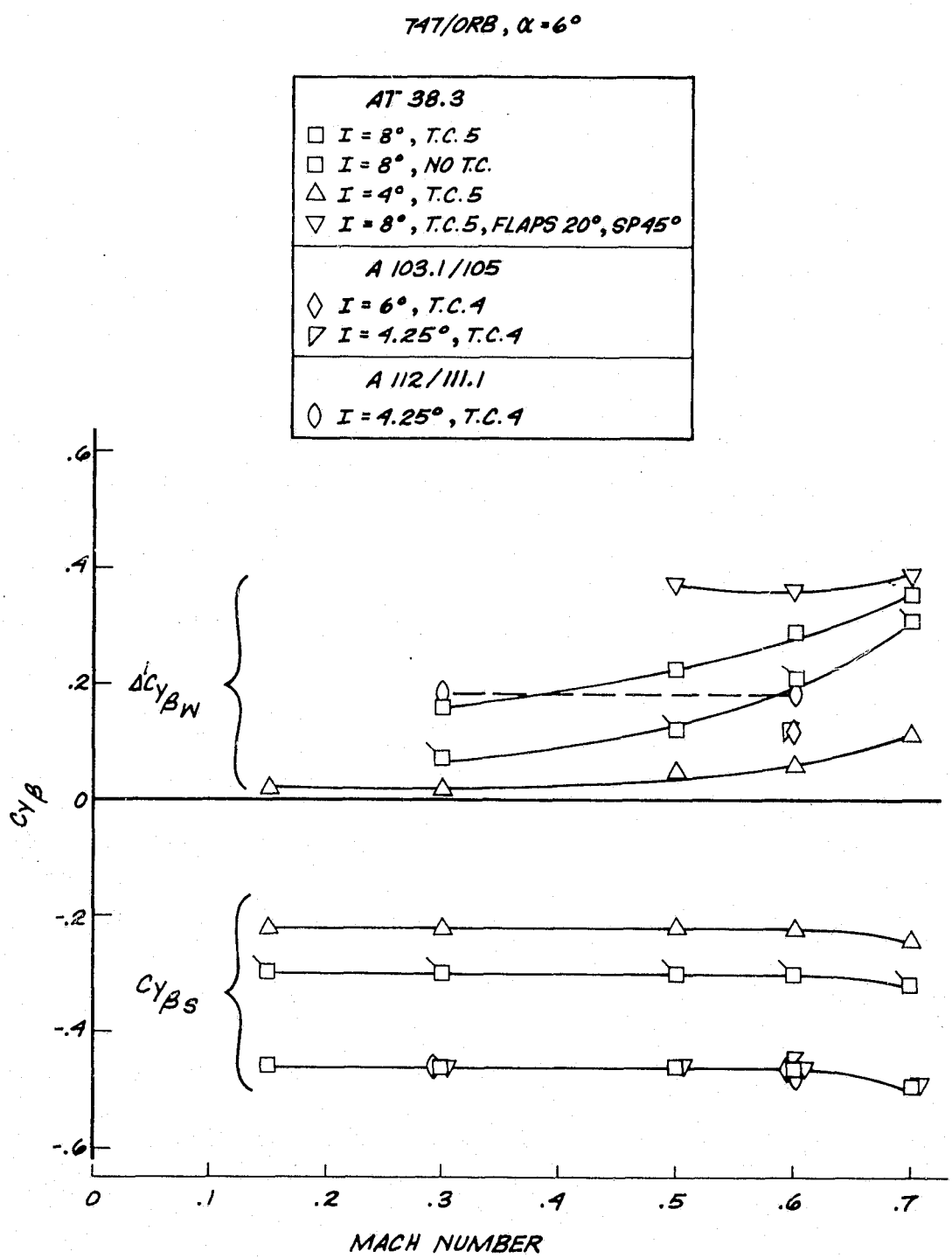


Figure 6 Local and Induced Derivatives for 747 Tail in Orbiter Wake

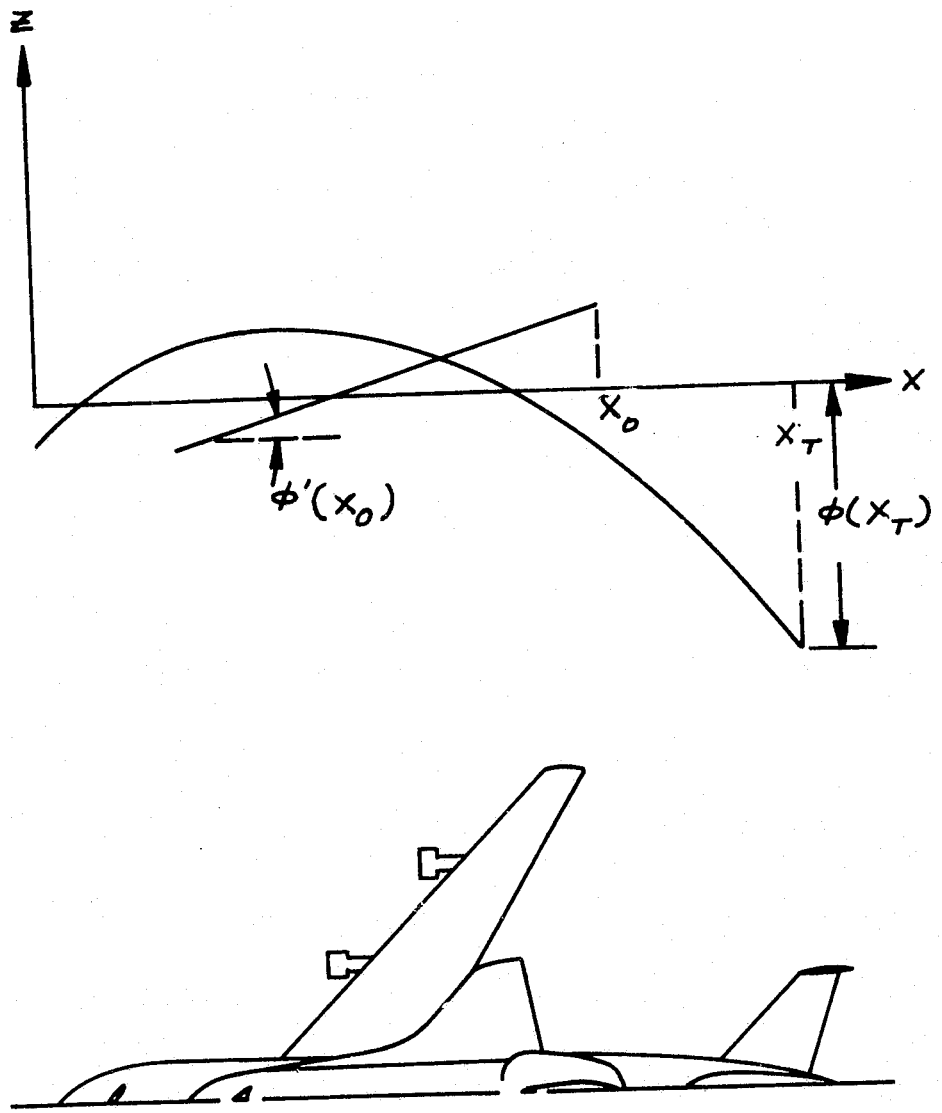


Figure 7 Coordinate System

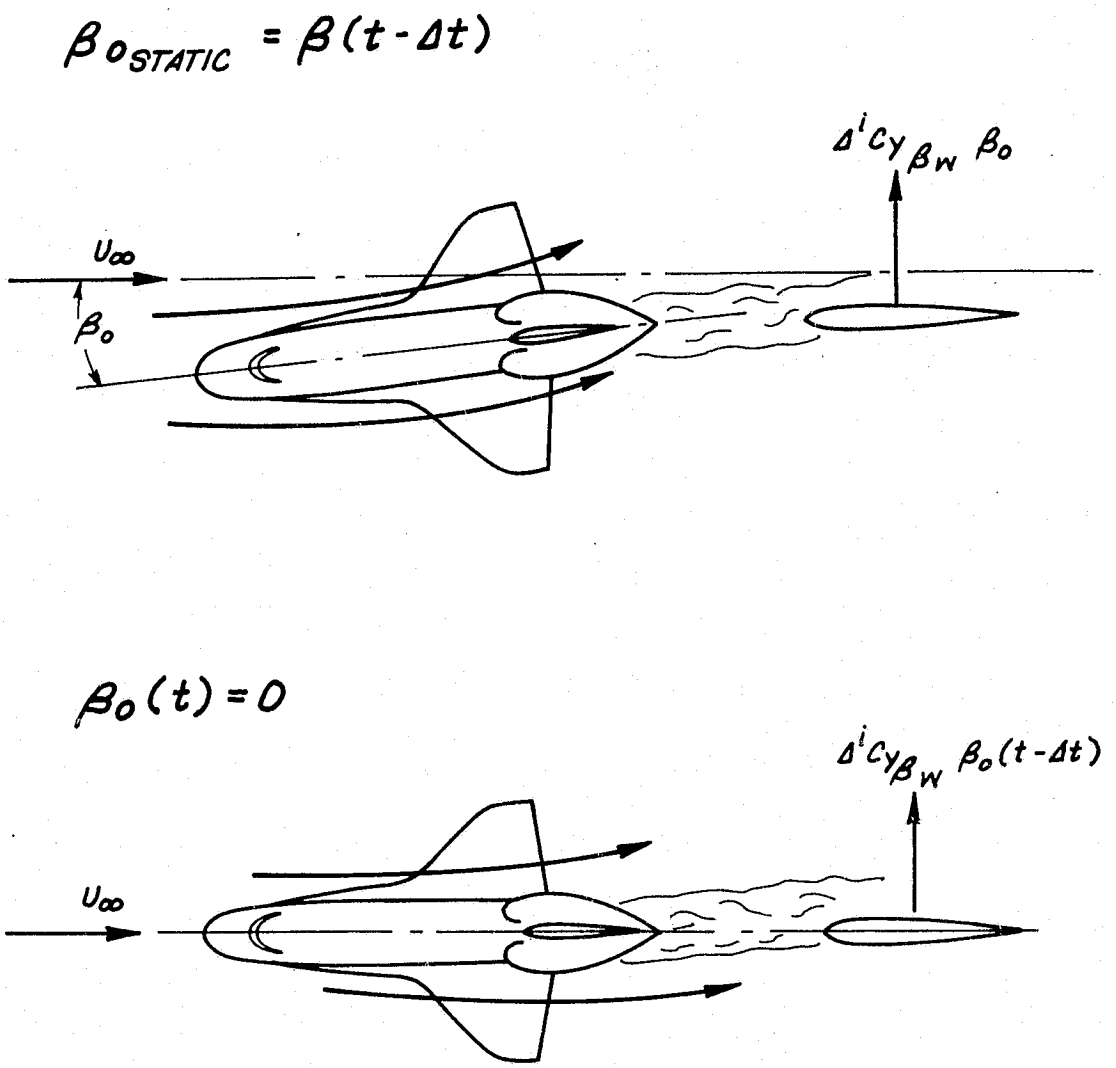


Figure 8 Quasi-Steady Loads on 747 Tail

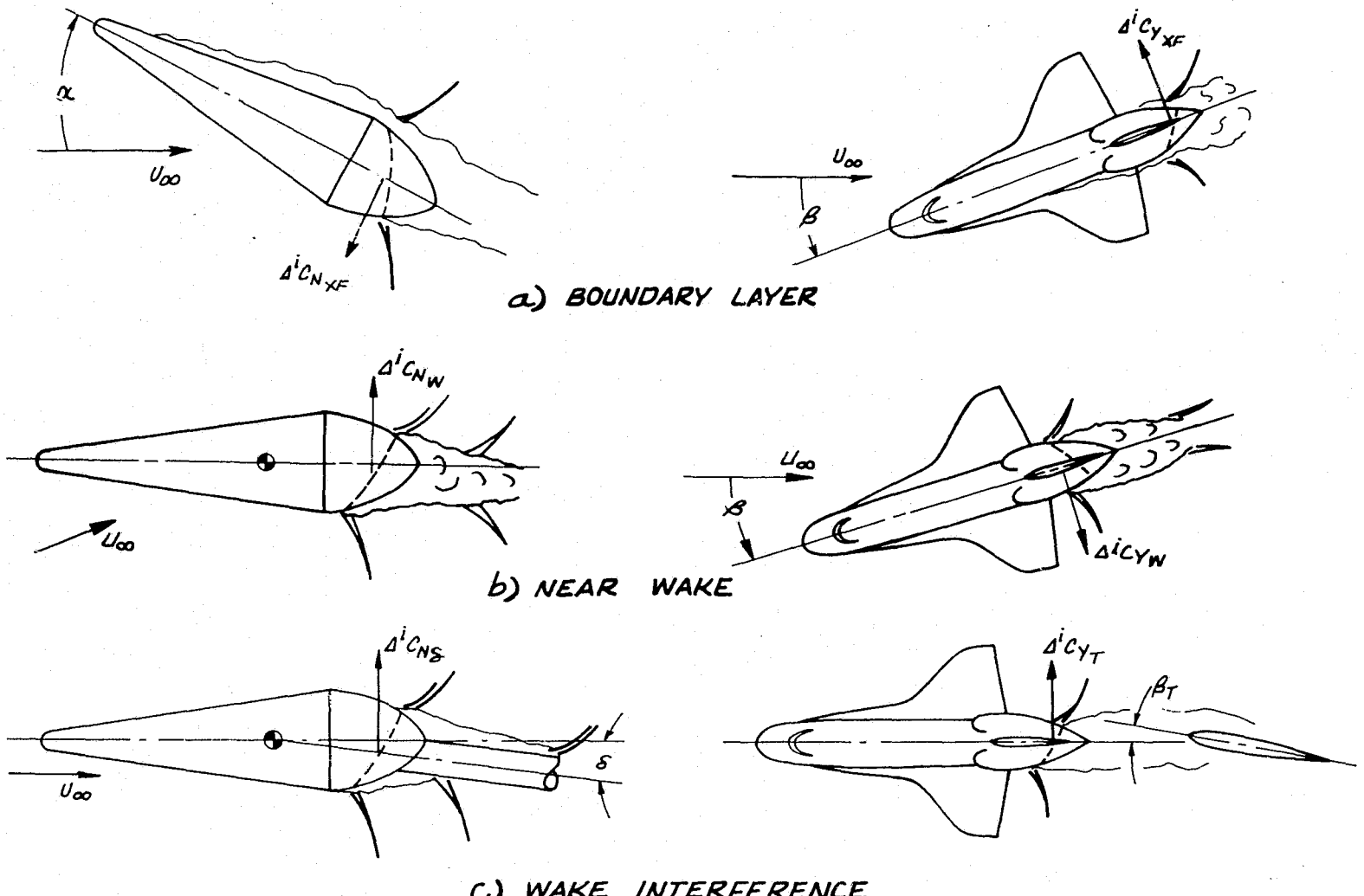


Figure 9 Quasi-Steady Loads on Orbiter Tail Fairing

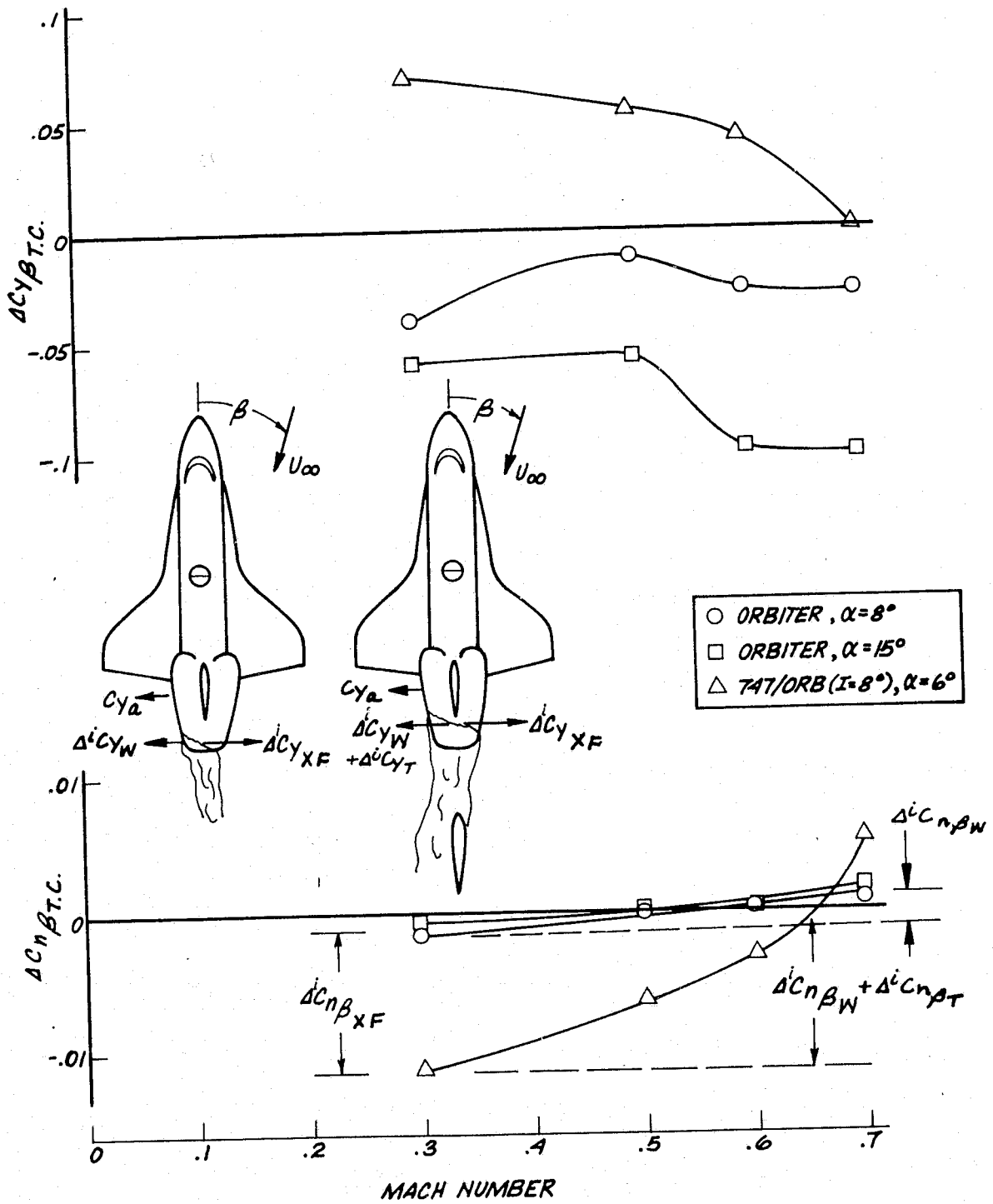


Figure 10 Induced Loads on Orbiter Beaver-Tail Tail Fairing T.C. 5

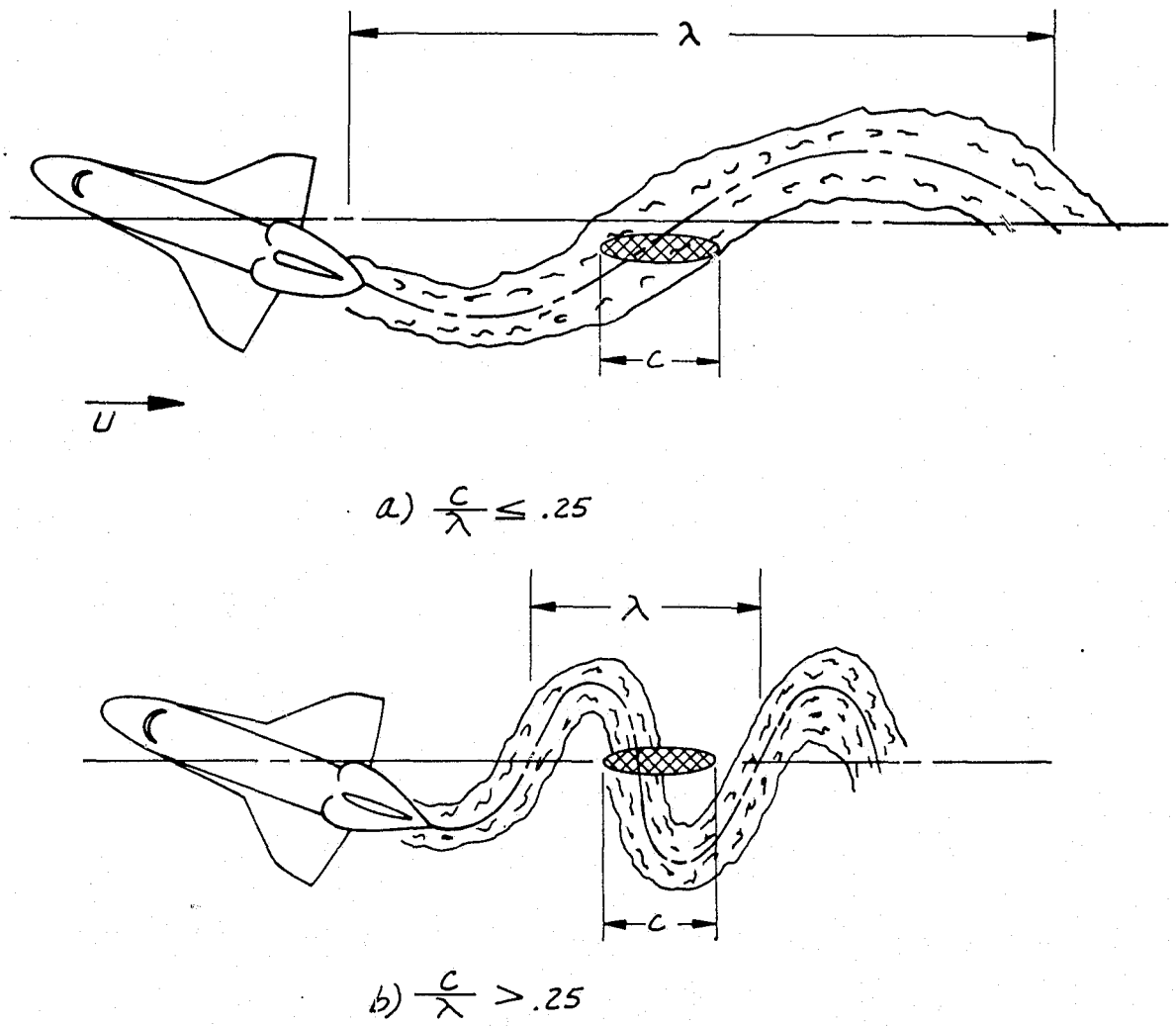


Figure 11 Limit of Quasi-Steady Theory

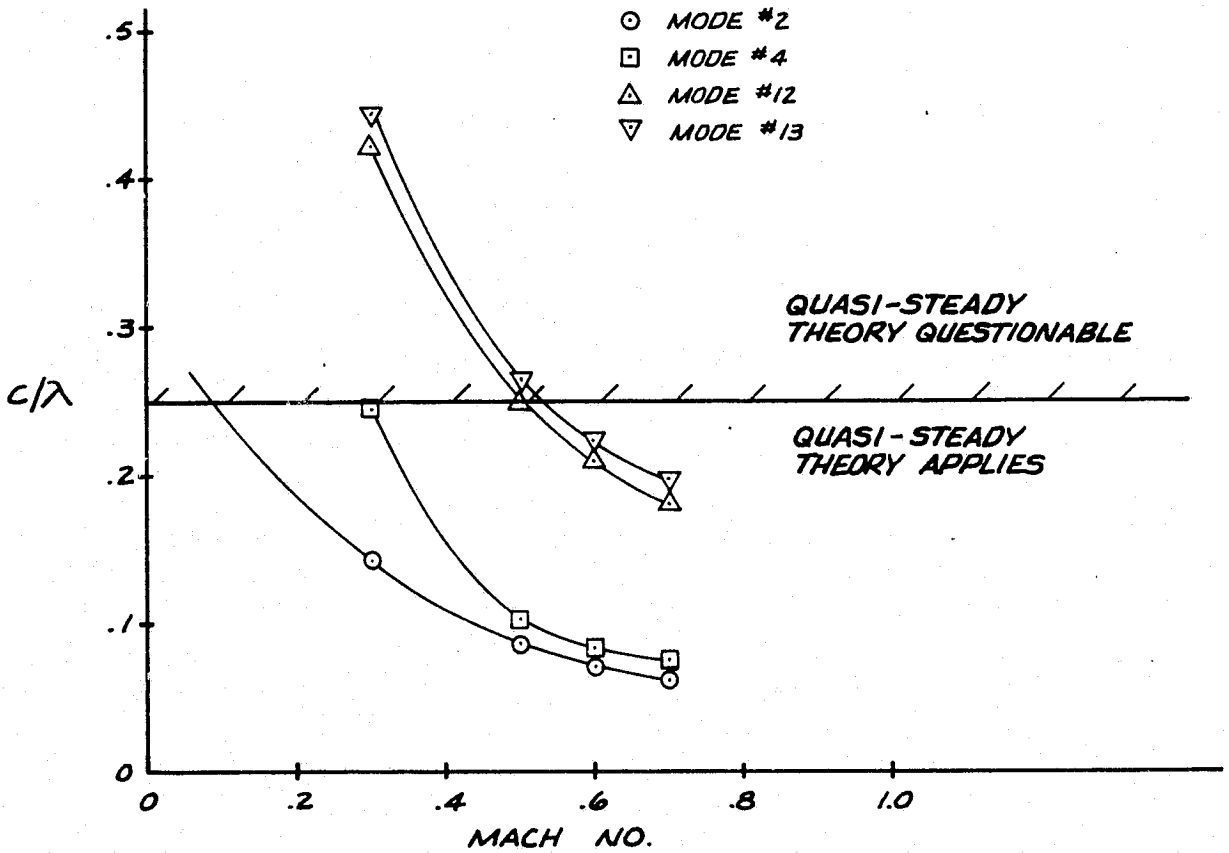


Figure 12 Limit of Quasi-Steady Theory for 747/Orbiter Antisymmetric Modes

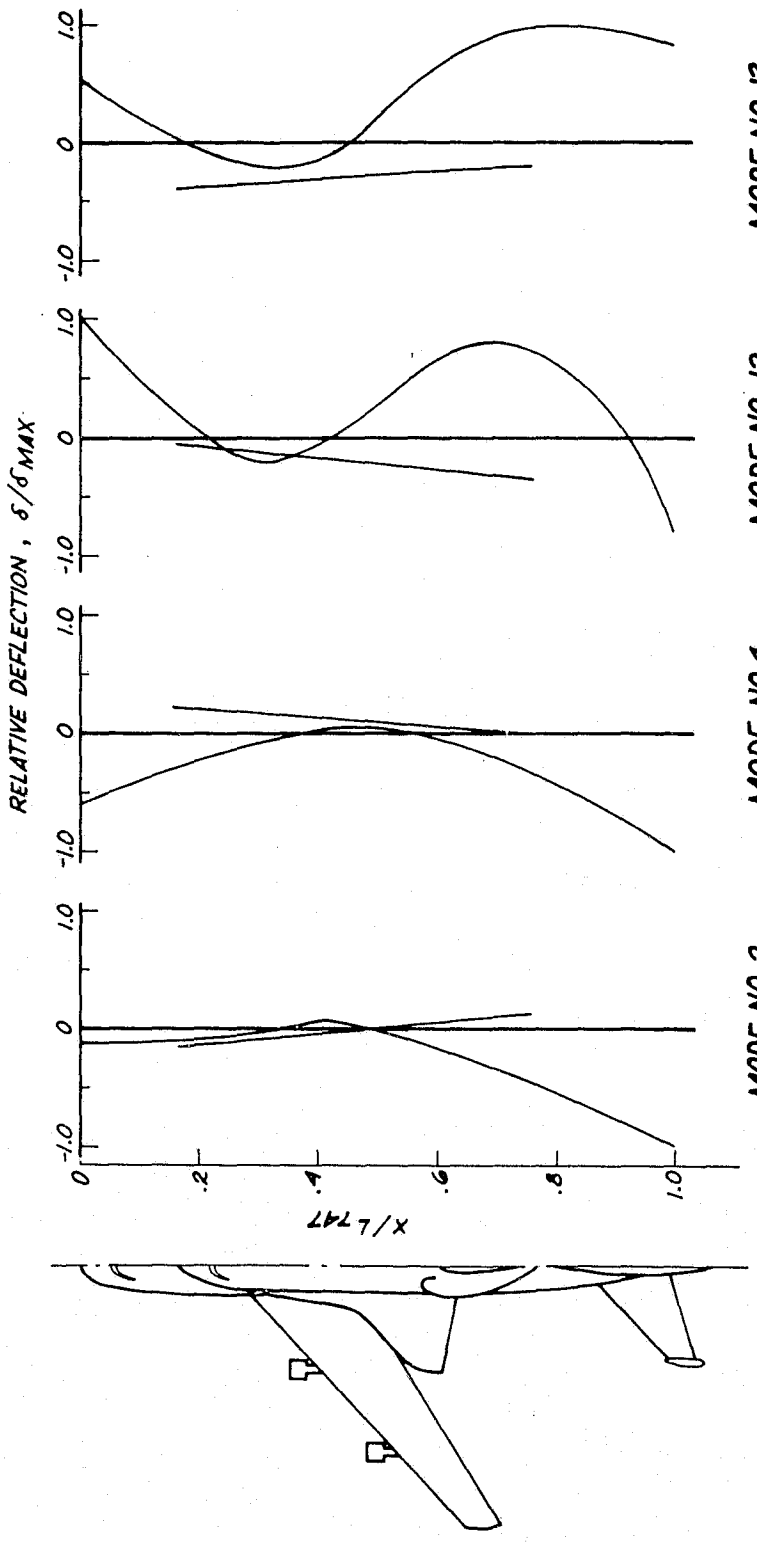


Figure 13 747/Orbiter Antisymmetric Modes

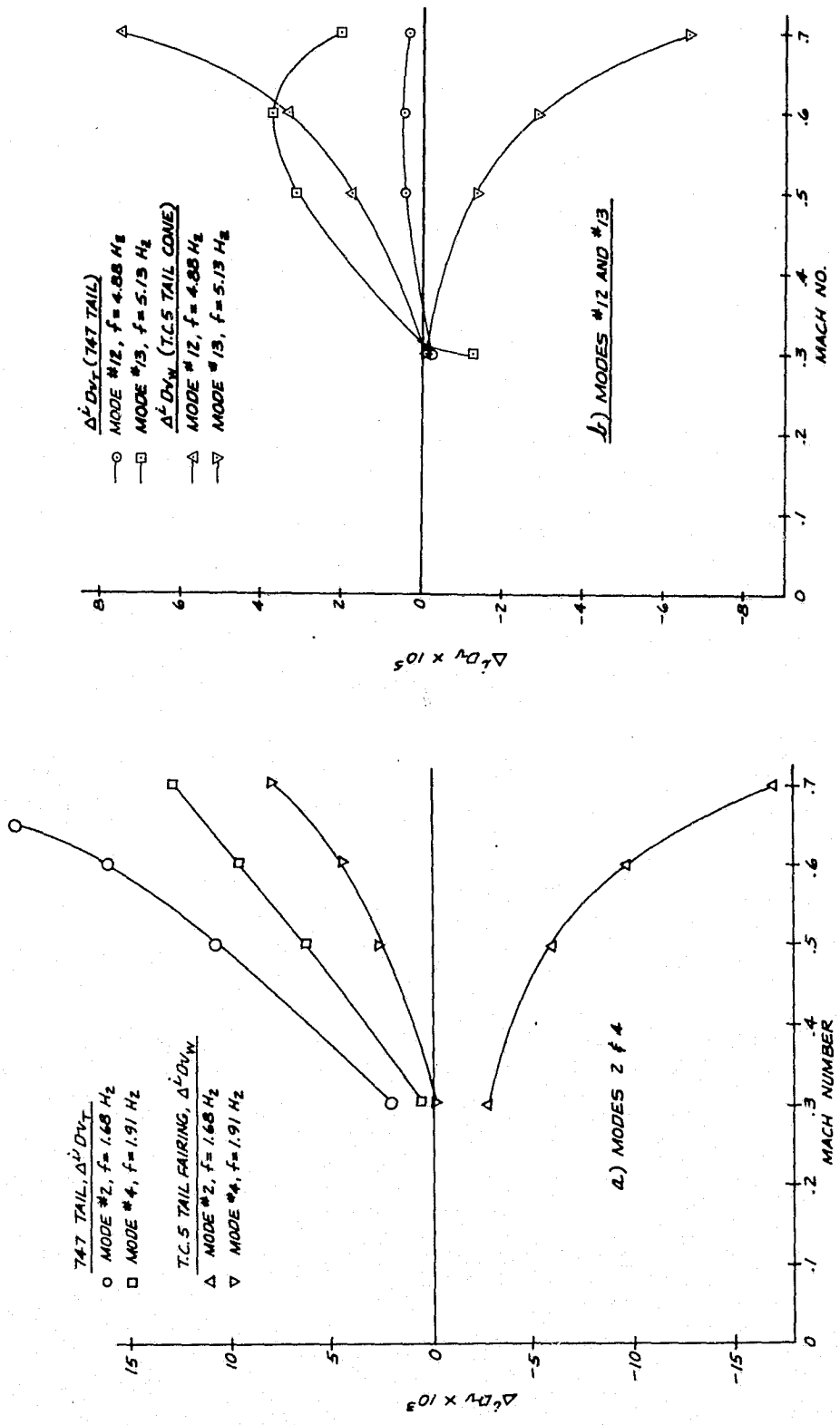


Figure 14 Relative Magnitude of Induced Damping Derivatives for 747/Orbiter; (I = 8°) T.C. 5, HT 38.3, $\alpha = 6°$

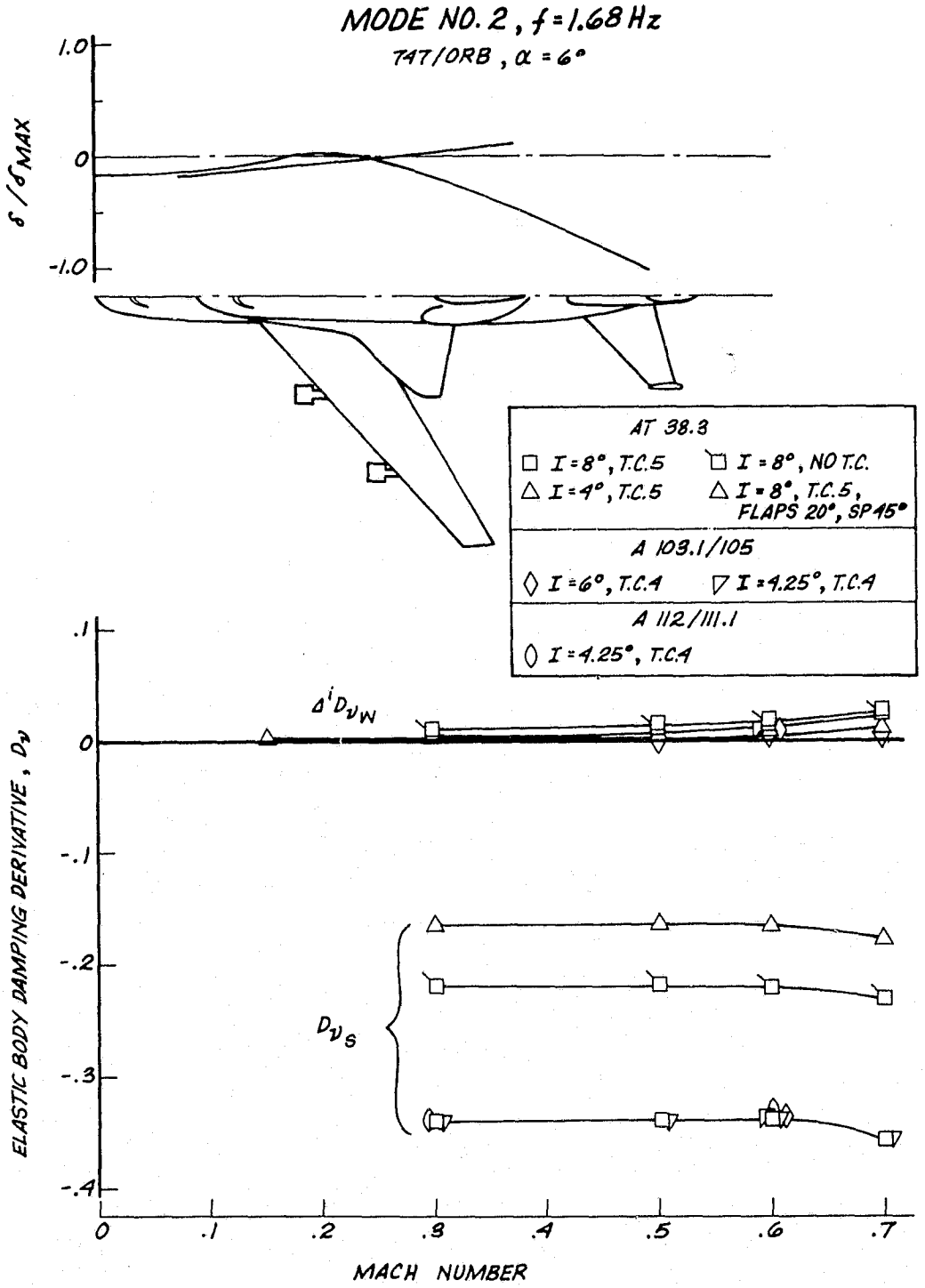


Figure 15 Elastic Body Damping Derivatives on 747 Tail for the Critical Antisymmetric Mode

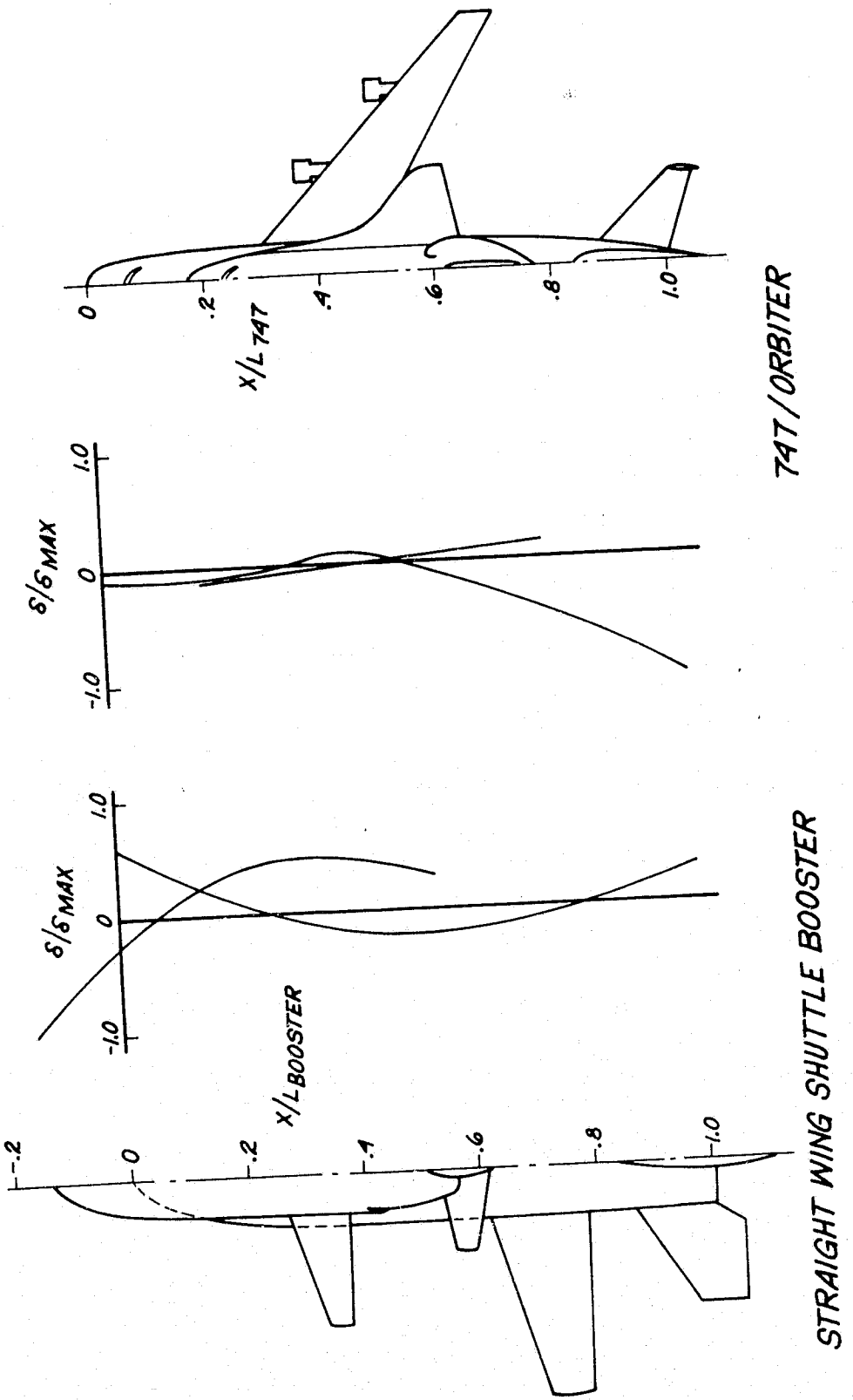


Figure 16 Comparison of Critical Modes

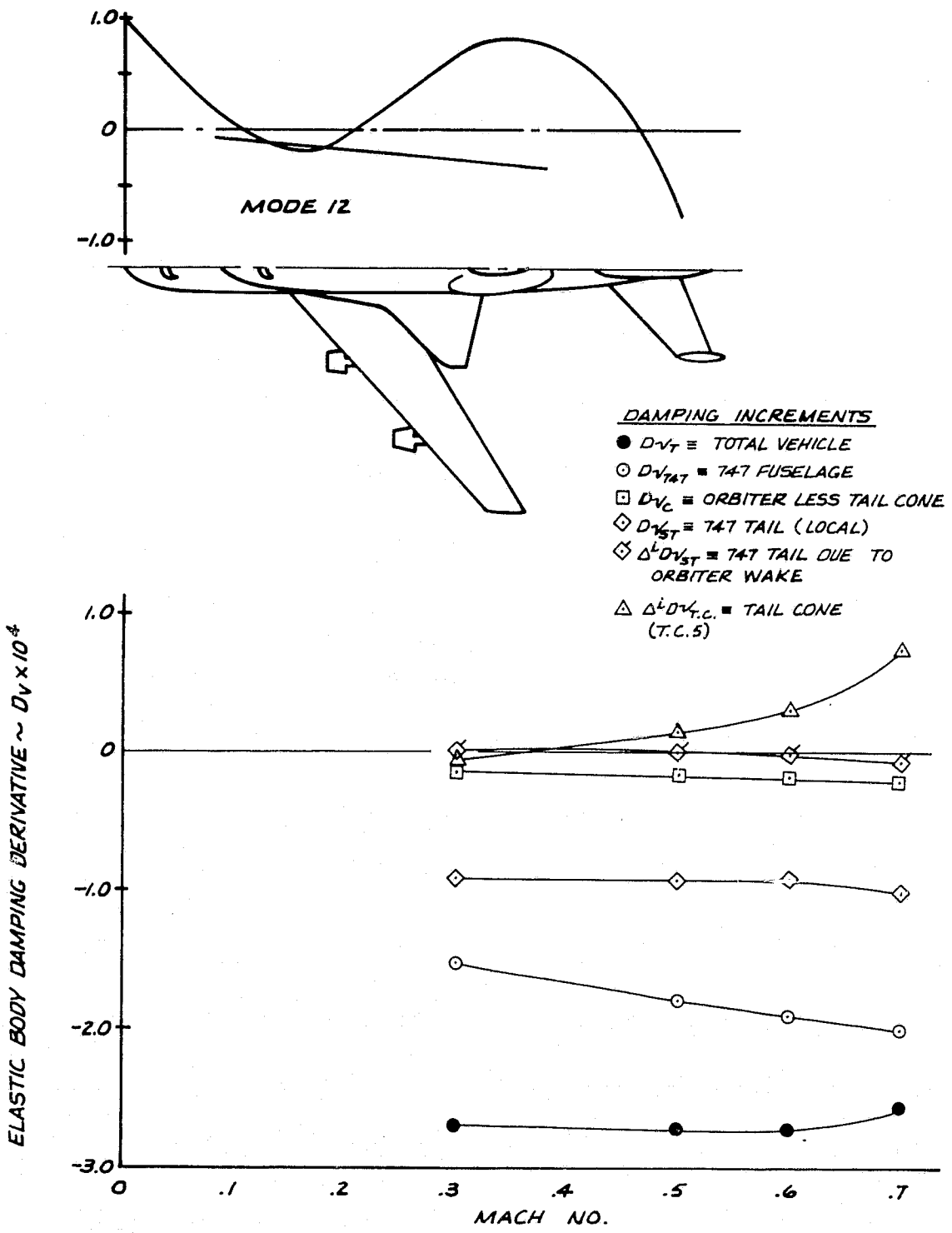


Figure 17 Elastic Body Damping Derivatives for Critical Tail Fairing Antisymmetric Mode (#12, f = 5.13 Hz, T.C.5)

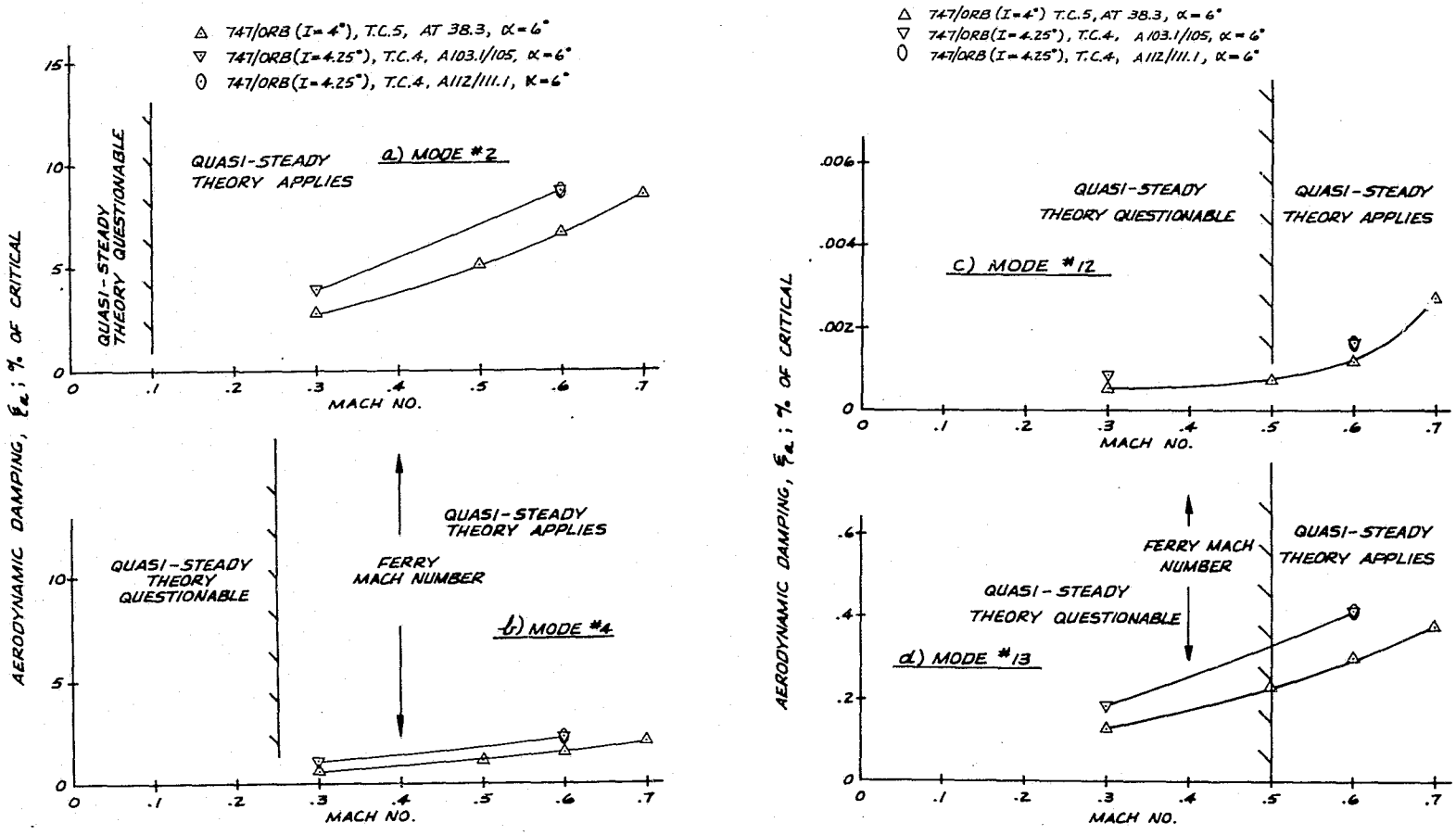


Figure 18 Aerodynamic Damping at Ferry Altitude (30,000 ft.)

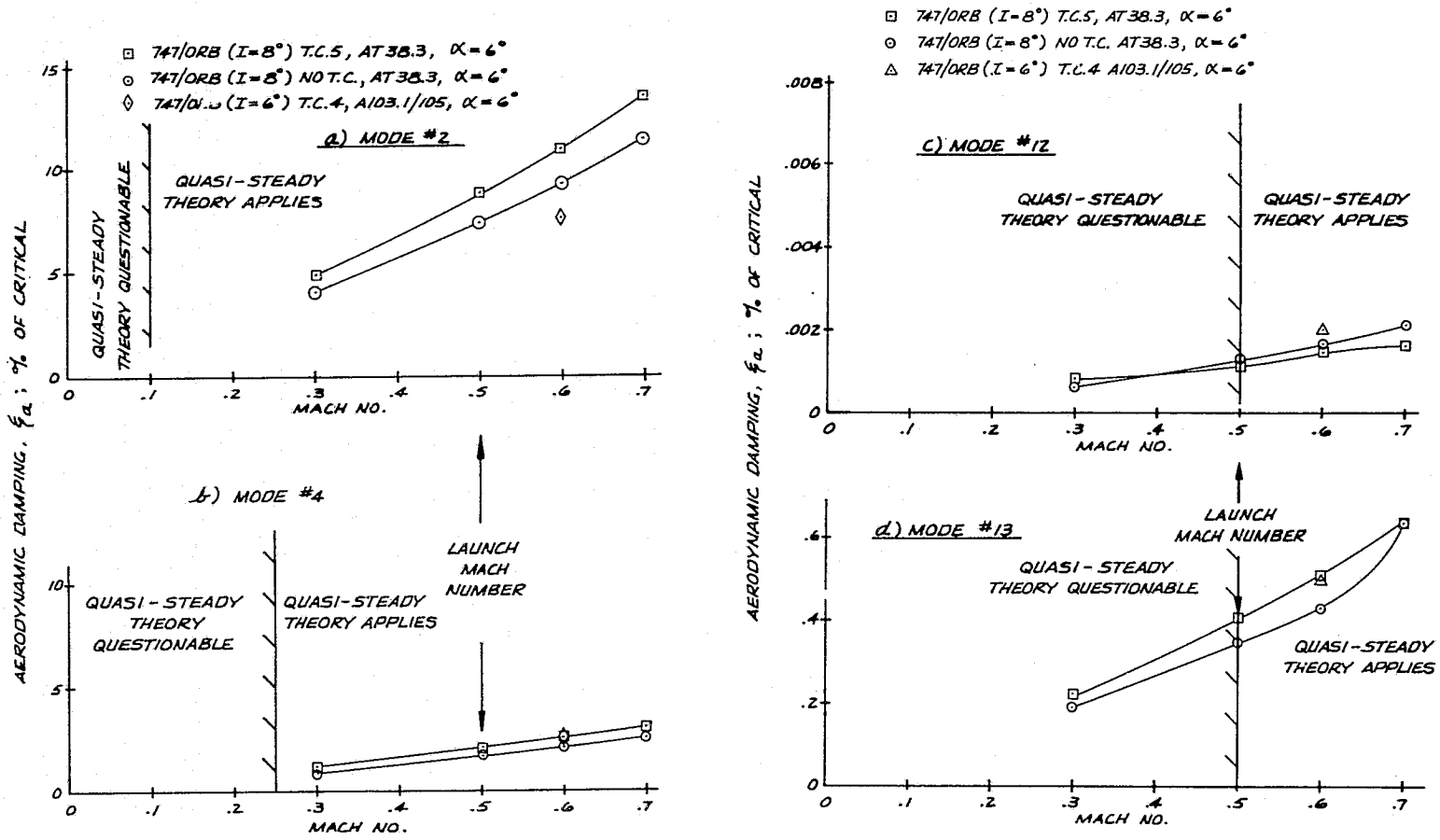


Figure 19 Aerodynamic Damping at Launch Altitude (25,000 ft.)

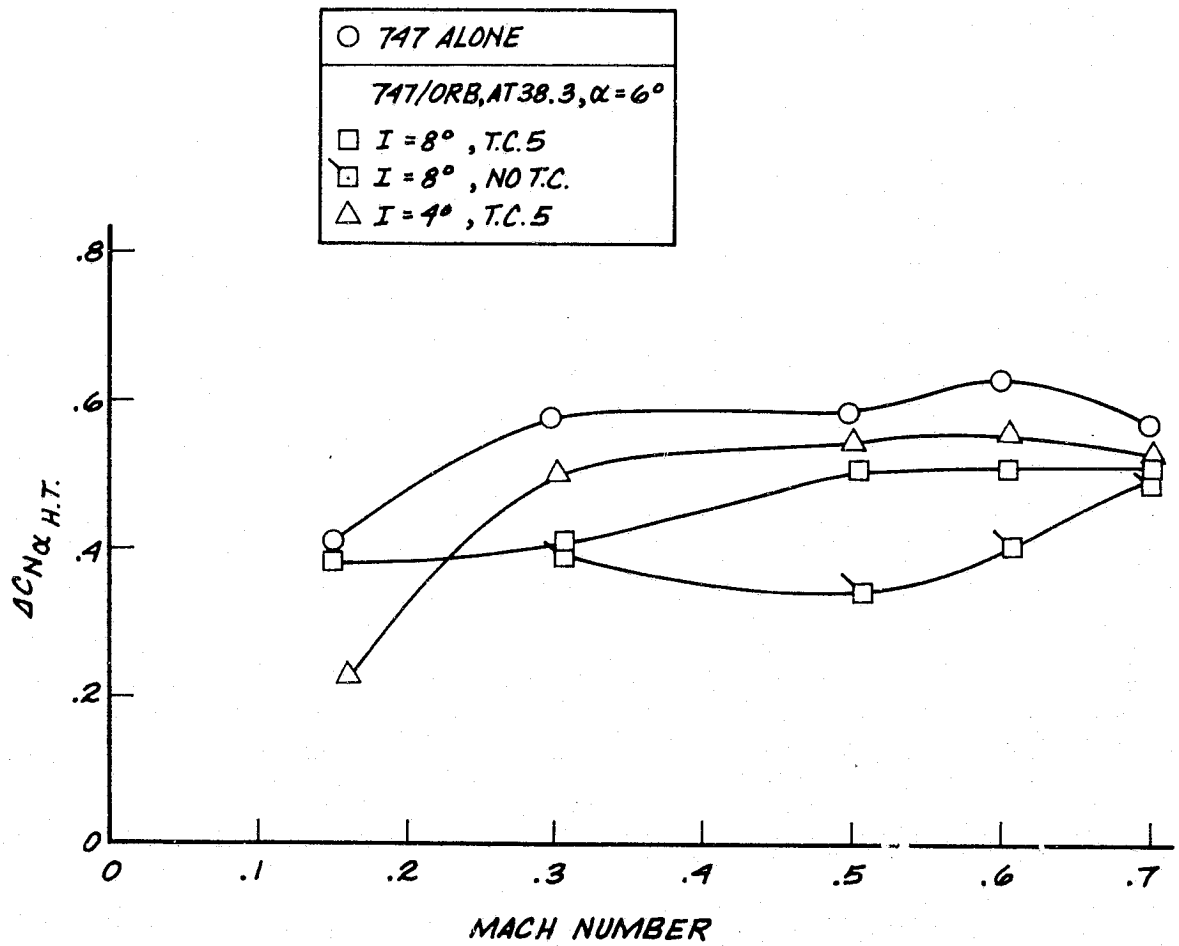


Figure 20 Effect of Orbiter Wake on 747 Horizontal Tail Load

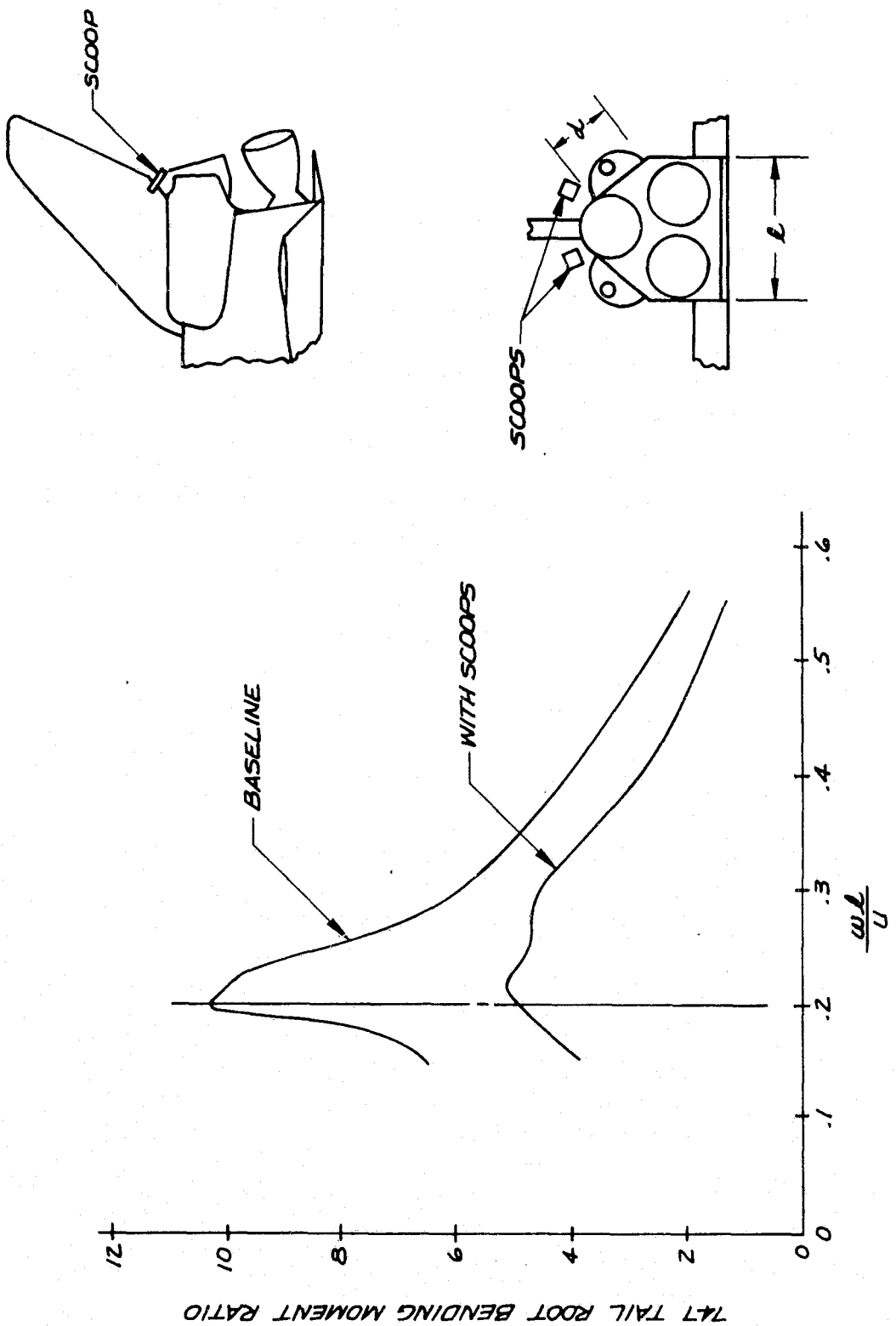


Figure 21 Effect of Scoops on 747 Tail Root Bending Moment

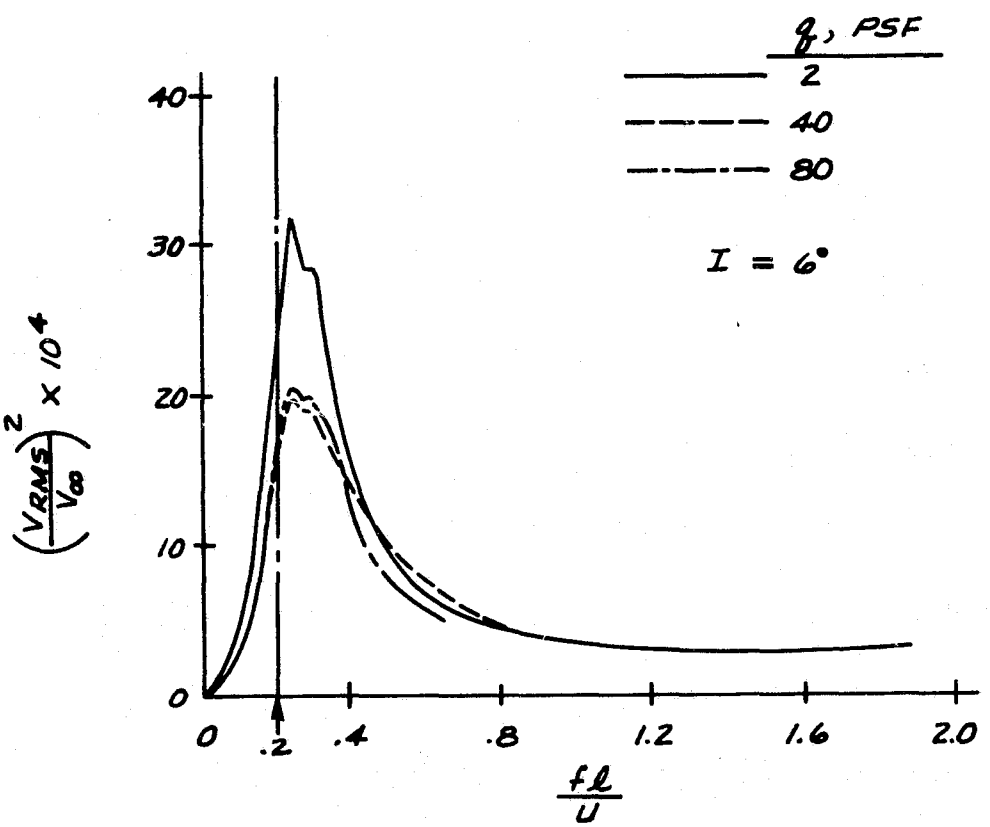


Figure 22 Effect of Dynamic Pressure on Fluctuating Velocity Ratio in the Orbiter Wake

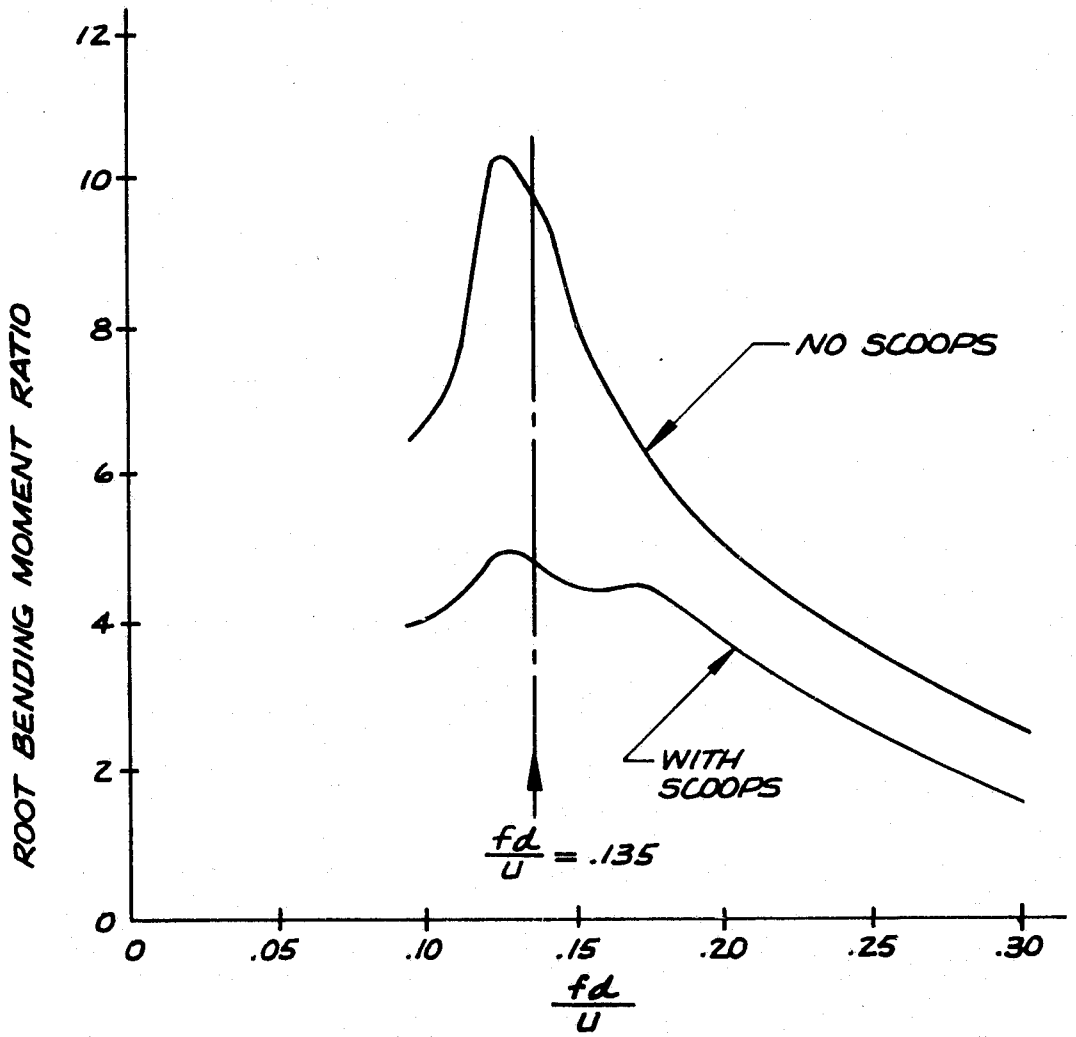


Figure 23 Correlation of Bending Moment Spectra with OMS Pod Characteristic Dimension

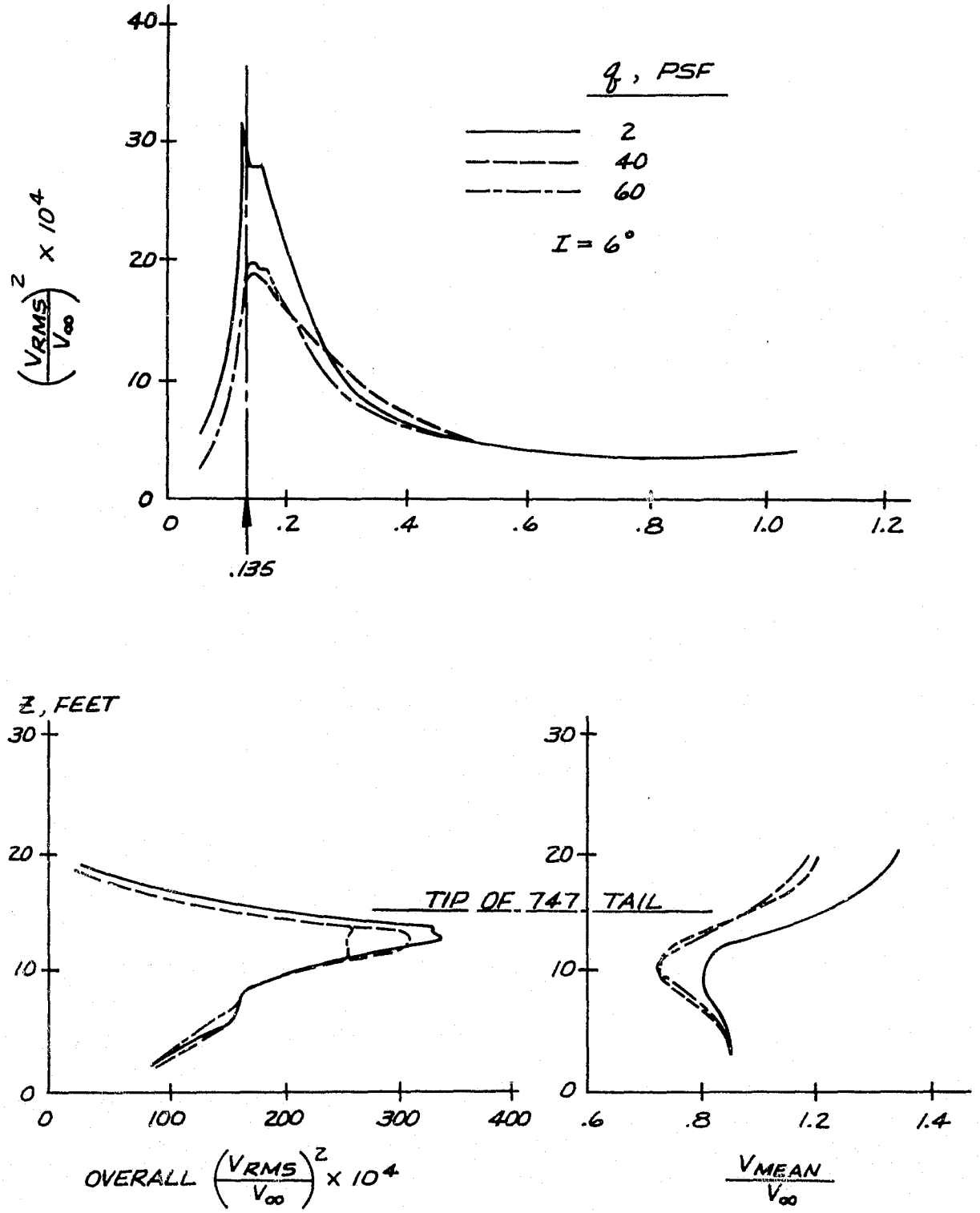


Figure 24 Correlation of Fluctuating Velocity Spectra with OMS Pod Characteristic Dimension

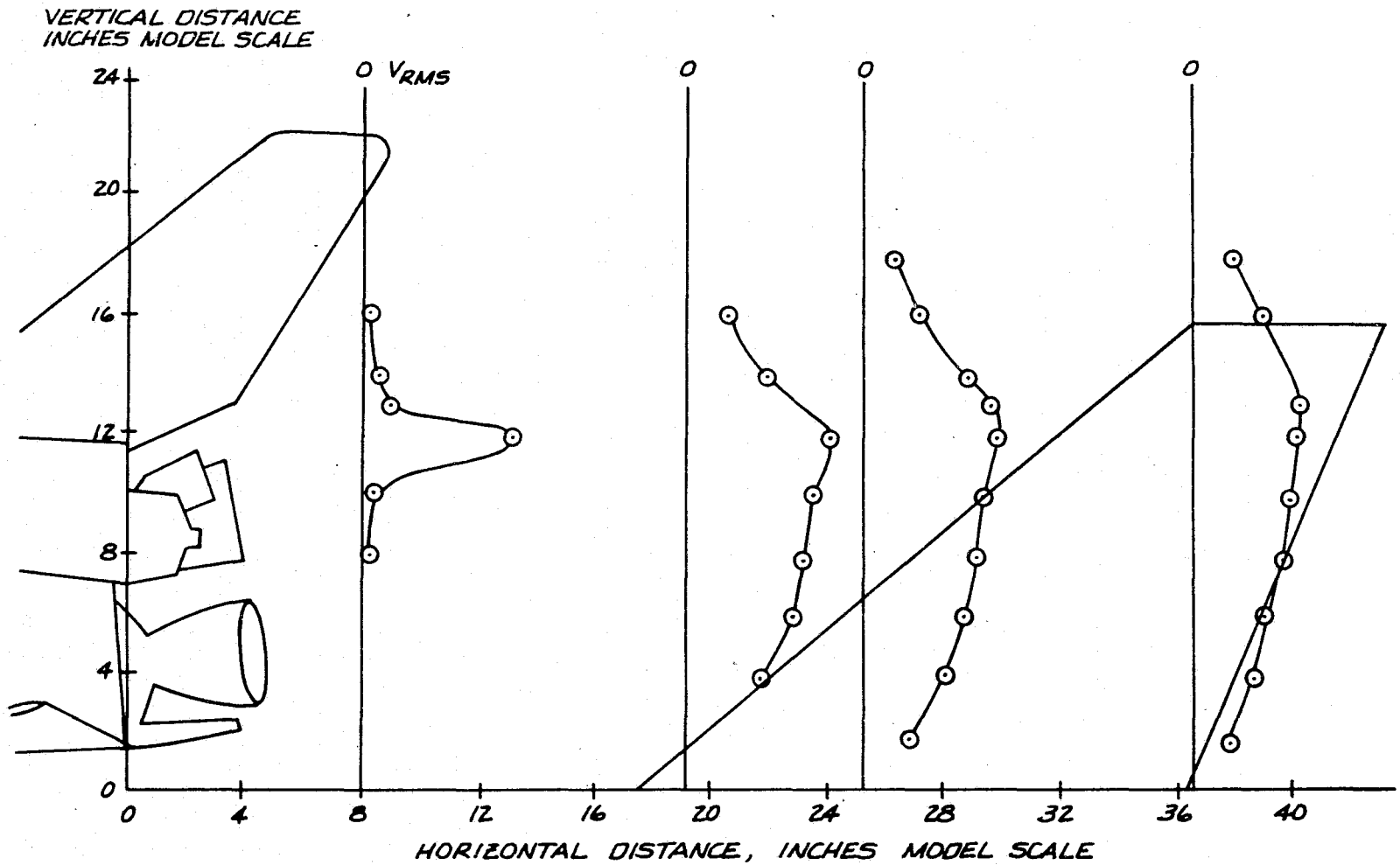


Figure 25 Fluctuating Velocity Profiles in Orbiter Wake

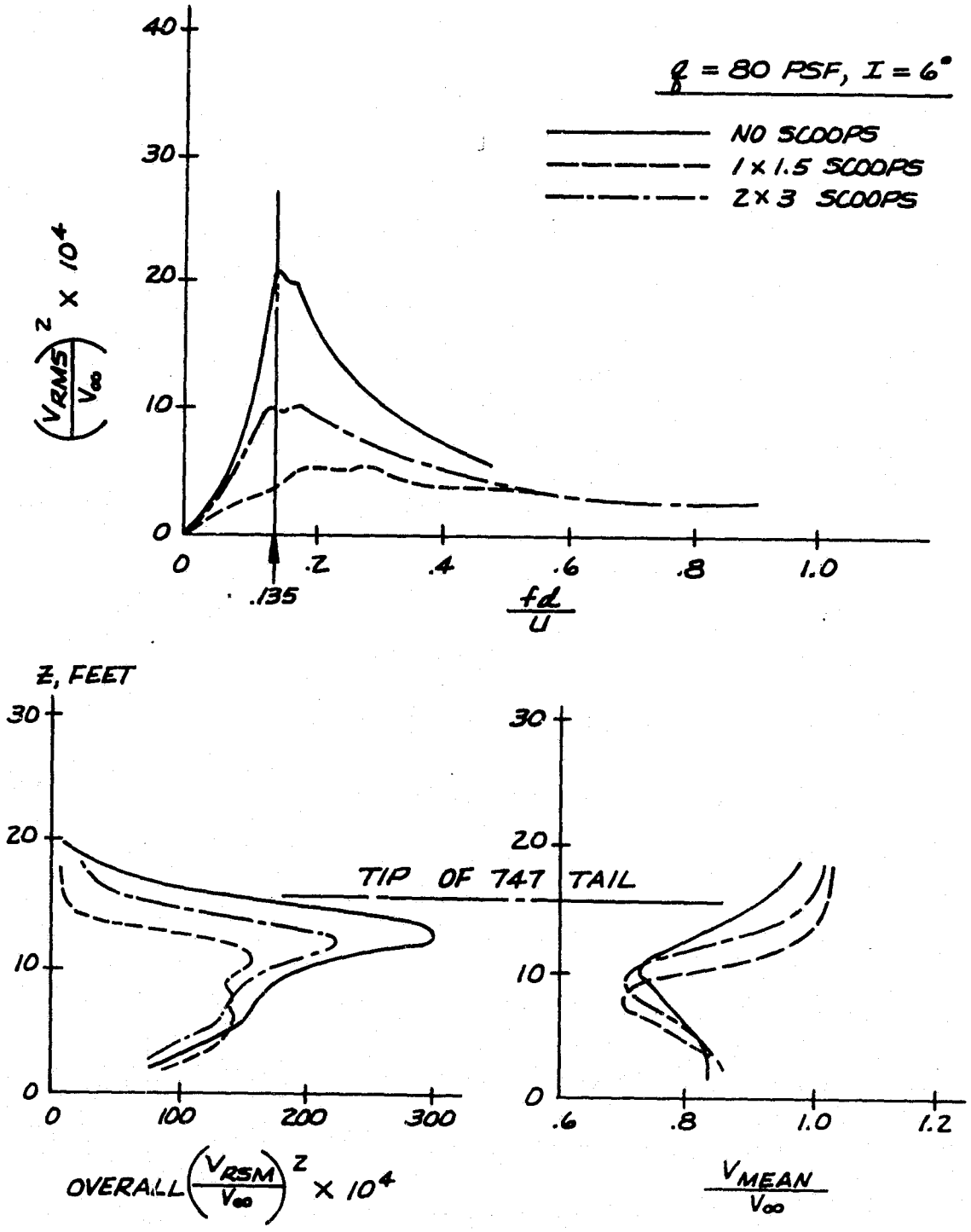


Figure 26 Effect of Scoops on Velocity Ratios

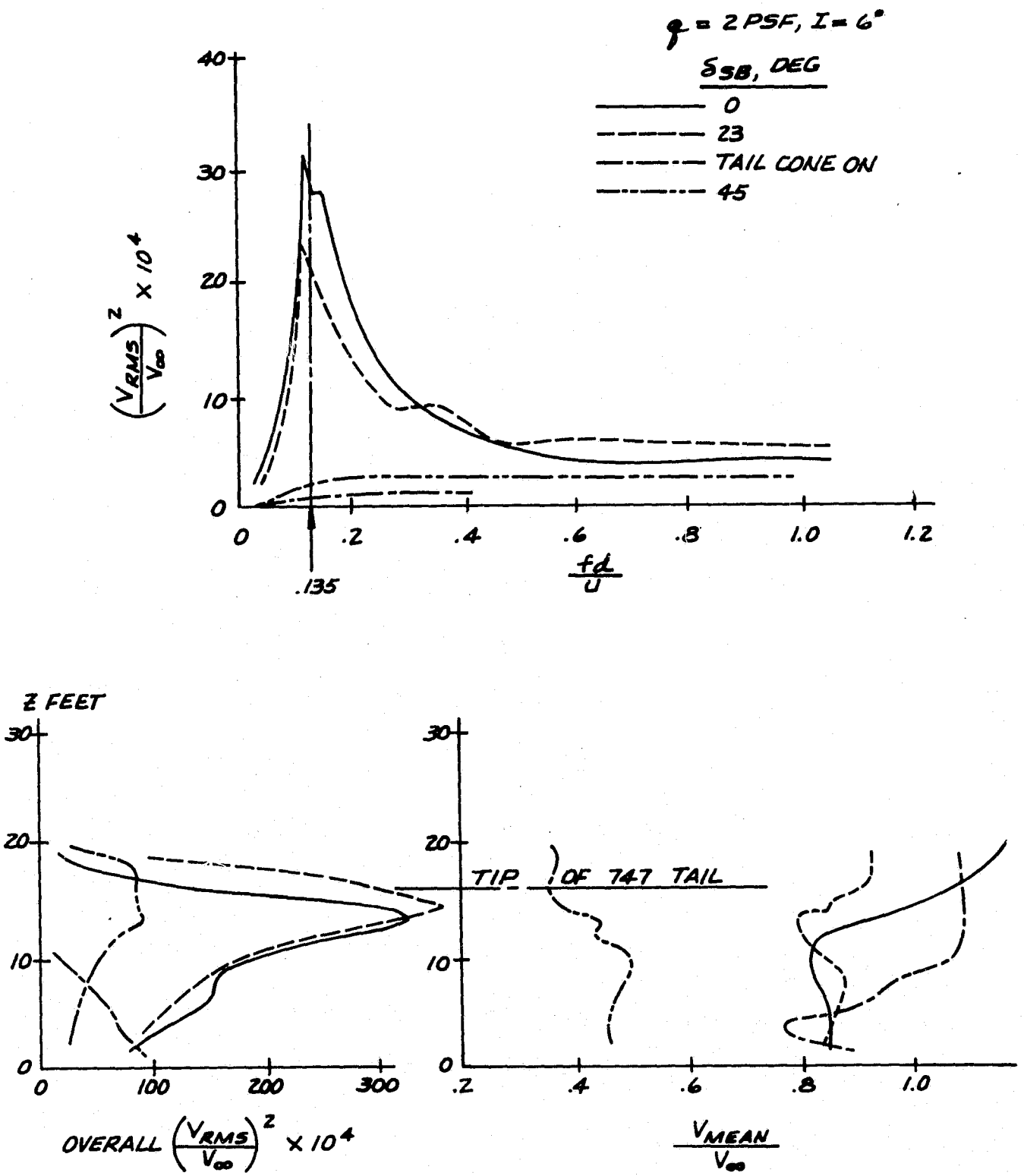


Figure 27 Effect of Speed Brake on Velocity Ratios

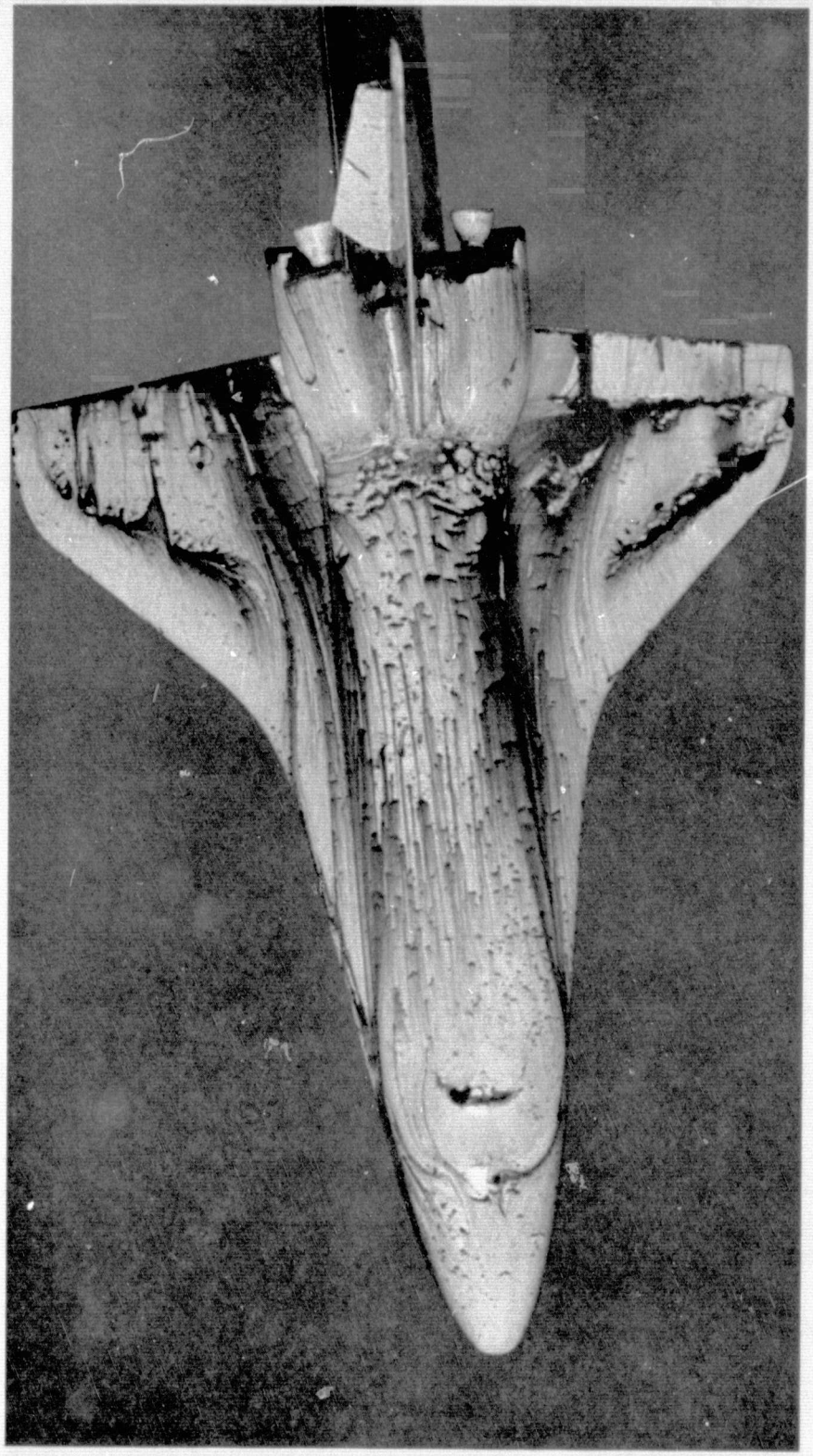

Figure 28 Effect of Speed Brake Deflection on OMS Pod Flow, M = 0.6

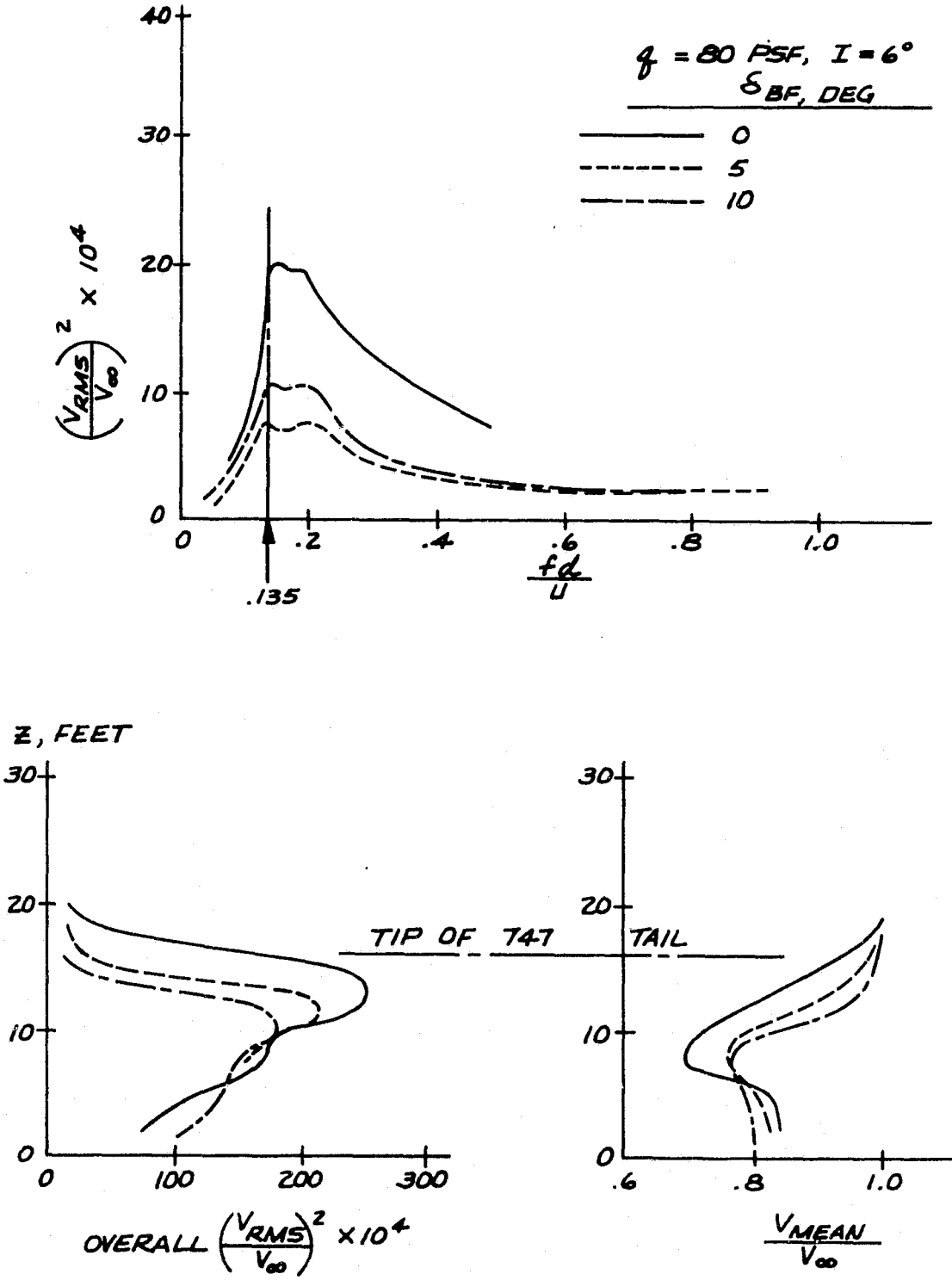


Figure 29 Effect of Body Flap on Velocity Ratios